A NUMERICAL STUDY OF THE EFFECTS OF INHOMOGENEOUS MEDIA IN DIFFUSION WEIGHTED IMAGING

By

Jessica Cervi

A Thesis Submitted in Partial Fulfillment

of the Requirements for the Degree of

Master of Science

in

The Faculty of Science

Modelling and Computational Science

University of Ontario Institute of Technology

July, 2015

Abstract

Diffusion Weighted Imaging (DWI) -a common Magnetic Resonance Imaging (MRI) technique - is used to infer material properties of tissues from the average diffusion of water molecules over brief time intervals. In particular, the Apparent Diffusion Coefficient (ADC), a measure of the magnitude of diffusion within tissues, can be derived from the MR signal under the assumption of homogeneous medium. Unfortunately, the complex structure of a typical volume element of physiological tissue contains many types of cells separated from extracellular space by semi-permeable barriers and is thus far from homogeneous.

In this thesis, we define an idealized tissue model as a system of cells separated by non-uniformly spaced semi-permeable membranes and extracellular space. Finite-difference solutions of the associated PDE model can be used to compute a Displacement Probability Density Function (DPDF). Having numerically computed the DPDF it is possible to simulate the intensity of the MRI signal and, from it, compute the ADC as in a real Diffusion Weighted-MRI experiment. The ADC is measured by averaging the second moments of the DPDF. Finally, we investigate the changes in the ADC in an inhomogeneous model by including higher order moments of the DPDF and we discuss the possible advantages of these alternative definitions.

Acknowledgements

> And those who were seen dancing
> were thought to be insane by those
> who could not hear the music.
>
> *F. Nietzsche*

Many thanks to my supervisors Dr. Greg Lewis and Dr. Dhavide Aruliah for their guidance, advice, precious help and encouragement until the very end of this project. I feel very lucky having had them as my advisors.

A precious thought goes to my parents, my brothers and their families, for supporting me and my passion during all this journey. I cannot forget my friends Catalina, Marco, Francesco, Matteo and many others for keeping a smile on my face even with an ocean between us. Thanks to all the people I met here: friends, staff and faculty members have been of great help. Of course, I cannot forget Kevin; he has been really great.

Finally, I want to thank Dr. Alberto Tagliaferro, Dr. Franco Gaspari and the people from the Italian Cultural Club of Durham (ICCD) for the encouragement, support, and for making this journey possible.

Author's Declaration

I declare that this work was carried out in accordance with the regulations of the University of Ontario Institute of Technology. The work is original except where indicated by special reference in the text and no part of this document has been submitted for any other degree. Any views expressed in the dissertation are those of the author and in no way represent those of the University of Ontario Institute of Technology. This document has not been presented to any other University for examination either in Canada or overseas.

Jessica Cervi

Date: July 15, 2015

Contents

List of Figures

List of Tables

Chapter 1

Introduction

1.1 Background

Diffusion MRI is a relatively recent branch of Magnetic Resonance Imaging (MRI) that has been used to produce information regarding human physiology and various porous structures. Diffusion MRI is applied [12] to infer structural information at a sub-voxel level by interpreting MRI signals [14].

In a broader sense, MRI is a well-known, non-invasive tomographic imaging technique for visualizing internal structures with a high degree of detail. MRI is able to produce images of internal physical and chemical characteristics of a system using nuclear magnetic resonance (NMR) [34]. The NMR phenomena was observed for the first time in 1846 by Bloch and Purcell [34]. However, it was not until 1972 that Paul Lauterbur developed the technology and the theory needed to encode spatial informations using NMR and build the first MRI scanner. Thanks to the deep physical theory behind the MRI modality, MR images are able to provide a rich variety of information. The image voxel value depends on a large set of intrinsic parameters that can be tuned to enhanced or suppress imaging effects. MRI is able to provide strong contrast between different types of soft tissues in the body and is widely used to image human brains, hearts, muscles, and even to locate tumours.

The first experiments to combine diffusion-weighted magnetic resonance measurements with MRI were published in 1984 [25]. However, in the past thirty years, developing and improving diffusion imaging techniques have become a research area of great interest due to established success in clinical neurodiagnostics [14].

1.2 Diffusion Magnetic Resonance Imaging Techniques

Various MRI-based diffusion imaging techniques have been developed since the earliest experiment combining diffusion theory with MRI. Diffusion MRI has been used to infer different kinds of information (e.g., tissue connectivity, anatomical features, etc.). The simplest imaging technique is Diffusion Weighted Imaging (DWI); this makes use of the variability of the Brownian motion that water molecules experience in tissues to map the changes in average magnitude of diffusion under the assumption of isotropy. Imaging techniques range from DWI, to other more complex techniques that are able to capture information in more than one dimension. Examples of these techniques include Diffusion Tensor Imaging (DTI), Diffusion Kurtosis Imaging (DKI), Q-ball imaging, and tractography [14]. In this thesis, we begin the discussion by introducing a fundamental component of all diffusion MRI schemes - the *Displacement Probability Density Function*.

1.2.1 Displacement Probability Density Function ρ

Before explaining the Displacement Probability Density Function, it is useful to introduce, briefly, some basic concepts of Probability theory, starting from the definition of a continuous random variable.

Notions about probability theory

A continuous random variable is a real-valued function that associates a unique numerical value to every, uncountably infinite, outcome of an experiment [18]. In particular, a random variable X is continuous if there exists a non-negative, integrable function $f(x)$ so that, for every set B,

$$P(X \in B) = \int_B f(x)dx, \tag{1.2.1}$$

where the function $f(x)$ is called the Probability Density Function (PDF) of X [15] and $P(X \in B)$ denotes the probability that X is on the set B.

The density function $f(x)$ must satisfy the following properties [7]:

1. $\int_{-\infty}^{+\infty} f(x)dx = 1$
2. $f(x)$ has to be non-negative on every set B, that is, $f(x) \geq 0$ for all x in B.
3. $\lim_{x\to-\infty} f(x) = 0$
4. $\lim_{x\to+\infty} f(x) = 1$

Additionally, the One crucial property of a continuous random variable is that $P(X = a) = 0$, if a is a specific event. This means that the probability of the exact event a happening is always zero. A simple way to think about this is by interpreting the probability density function as a curve; this means that, finding the probability that a continuous random variable X falls in some interval of values, involves finding the area under the curve $f(x)$ between the endpoints of the interval

$$P(a \leq X \leq b) = \int_a^b f(x)dx. \tag{1.2.2}$$

Clearly, if we consider an interval that is just the point corresponding to the event a, then, in the sense of the Riemann sum, the area under $f(a)$ is zero (i.e., $\int_a^a f(x)dx = 0, \forall x \in \mathbb{R}$). Because we cannot associate a probability to any precise value, we need a function to measure the probability that X falls into a certain interval a, b. For this reason we define the Probability Distribution Function as [15]

$$F(x) = P(X \leq x) = \int_{-\infty}^{x} f(s)ds, \tag{1.2.3}$$

where s in this case is a dummy variable. It is worth mentioning that $F(x)$ is an increasing function ($F(x) \leq F(y)$ is $x \leq y$).

It is important to say that the probability distribution function is a *probability* (i.e., its value is a number between zero and one), and it is defined for both discrete and continuous random variables. On the other hand, the probability density function contains information about probability of all the events, but is not a probability because it can assume any positive value, even a value larger than one.

Some characteristics of the shape of a continuous PDF can be described by certain quantities, called standardized moments. The n^{th} moment of a real-valued continuous

function $f(x)$ about a value c is defined as

$$\mu_n = \int_{-\infty}^{+\infty} (x-c)^n f(x) dx. \tag{1.2.4}$$

Given the definition for the moments, we can define the moment generating function $M_X(\zeta)$ for a continuous random variable X as [15]

$$M_X(\zeta) = \mathbb{E}(e^{\zeta X}) = \int_{-\infty}^{+\infty} e^{\zeta x} f_X(x) dx, \qquad \zeta \in \mathbb{R}, \tag{1.2.5}$$

where $f_X(x)$ is the PDF for the random variable X and $\mathbb{E}$ is the expectation of $e^{\zeta X}$. By expanding (1.2.5) in Taylor series we can rewrite this as

$$\begin{aligned} M_X(\zeta) &\simeq \mathbb{E}[1 + \zeta X + \frac{1}{2!}\zeta^2 X^2 + \frac{1}{3!}\zeta^3 X^3], \\ &= 1 + \zeta \mathbb{E}(X) + \frac{1}{2}\zeta^2 \mathbb{E}(X^2) + \frac{1}{3!}\zeta^3 \mathbb{E}(X^3), \\ &= 1 + \zeta\mu_1 + \frac{\zeta^2 \mu_2}{2!} + \frac{\zeta^3 \mu_3}{3!} + \cdots, \end{aligned} \tag{1.2.6}$$

where $\zeta^n/n!, n = 1, \ldots, \infty$, are the coefficients of the expansion of $e^{\zeta x}$ in the moment generating function. In (1.2.6), the expectation of the n^{th} power of the random variable X, $\mu_n = \mathbb{E}(X^n)$, is the n^{th} moment of the random variable X.

The lower-order moments have recognizable names and are easy to compute. In particular, the first moment is the mean or the expected value, the second moment is the variance, the third moment is the skewness and the fourth moment is the kurtosis. The mean is used to refer to one measure of the central tendency either of a probability distribution or of the random variable characterized by that distribution. The variance is a measure of how spread out the values about an event are, and always has a non-negative value. For example, a variance of zero indicates that all the values associated with X are identical. We can think of the skewness as a measure of the asymmetry of the probability density function. The last moment we will introduce for our study is the kurtosis K: it is a descriptor of the shape of a probability density and it characterizes how peaked the probability density of a real-valued random variable is.

Having clarified some basic concepts of probability theory, we can introduce the notion of Displacement Probability Density Function (DPDF) and start interpreting it for cellular diffusion processes. The DPDF $\rho(x_0|x,t)$ is the PDF that a particle

starting at x_0 at $t = 0$ is at position x at time t, i.e., the probability that a particle starting at x_0 is between x_1 and x_2 at time t is

$$P(x_1 < X < x_2) = \int_{x_1}^{x_2} \rho(x_0|x,t)dx. \tag{1.2.7}$$

In diffusion MRI, water molecules are the particles of primary interest because water is a major constituent of biological tissue. Because of this reason, MRI is tuned to receive signal from the protons of water molecules. However, determining the form of the displacement density for such particles is very difficult due to the multitude of natural barriers to water diffusion, such as cell membranes organelles, plasma, membranes, and fibre tracts. These barriers make the diffusion of water an inhomogeneous random process. That is, the shape of the DPDF depends on x_0, the point where the particle starts diffusing.

In fact, in a homogeneous medium, the displacement PDF computed at one specific location in the domain would be the same under translation to any other location in the domain. In a homogeneous domain, the displacement density is a Gaussian (bell-shaped) function. In the case where diffusion in more than one direction is considered, the Gaussian is multivariate and corresponds to either isotropic (equal diffusion coefficients in all directions, Figure 1.1a) or anisotropic diffusion where there may be preferred directions of diffusion (Figure 1.1b). It is easy to understand that,

(a) Isotropic diffusion

(b) Anisotropic diffusion

Figure 1.1: Water diffusion in ordered structures exhibits directional preference depending on the geometry of the media itself. If the molecules are not likely to diffuse in any particular direction then the medium is said to be isotropic (a). If the structures permit molecules to diffuse more readily in one direction as opposed to others the medium is said to be anisotropic.(b).

in reality, the complex heterogeneity of biological tissue implies that the DPDF is, in general, not Gaussian. However, very often, due to the complexity of modelling these

elaborate structures, scientists make the simplifying assumption that there are no barriers or obstacles to water diffusion and, therefore, the medium can be considered homogenous. In the next section, we will discuss this assumption in the diffusion imaging techniques considered in this thesis.

1.2.2 Diffusion Weighted and Diffusion Kurtosis Imaging

In order to infer information about the biological microstructures from the MR signal, the most commonly used imaging techniques use the hypothesis of homogeneity across the whole domain to approximate the Displacement PDF of water molecules diffusing over a fixed period of time. It follows that, often, diffusion-based imaging techniques assume that diffusion follows a Gaussian distribution. This would be a very accurate description if the medium was homogenous. However, biological tissue are highly heterogenous. For example, the presence of cell membranes make biological diffusion media inhomogeneous [14] and, therefore the shape of the probability function of molecular displacement will depend on the molecules starting point [27]. This is true because, the diffusing molecules will encounter different kinds of obstacles depending on how close it starts to these obstacles. Because of the complexity that characterizes the tissue structures, the diffusion obstructed by the barriers and the obstacles in the medium is understood as an average of different probabilities over the entire sample.

The great attraction and interest in some imaging schemes, such as DWI, Diffusion Tensor Imaging (DTI) and Diffusion Kurtosis Imaging (DKI), lies in their simplicity and short acquisition times compared to more complex methods such as Diffusion Spectrum Imaging (DSI)[14]. In Diffusion Weighted Imaging, it is common practice to use a specific, one directional, MRI spin-echo sequence (see Section 3.1) tailored to acquire diffusion-weighted images [27]. By measuring the MRI signal in each voxel from such a sequence, it is possible to infer information about the biological tissue by computing the Apparent Diffusion Coefficient which is related to the 2nd-order moment of the PDF (see Section 3.2). Some common clinical applications of DWI include stroke localization [25] and characterization of renal and musculoskeletal diseases [27].

Despite these remarkable accomplishments, DWI fails to fully utilize the MR diffu-

sion measurements by implicitly assuming that the water molecule diffusion occurs in a free and homogeneous environment. To probe and characterize the non-Gaussian diffusion, a new imaging technique called Diffusion Kurtosis Imaging (DKI) has been developed recently [33]. In theory, DKI aims to provide a higher-order description of the restricted water diffusion process by gathering information from the 2^{nd}- and 4^{th}-order moments of the Displacement PDF. DKI findings are promising. Measurements of the apparent kurtosis along the diffusion gradient encoding directions have been demonstrated to offer a better and improved understanding of neural tissue changes [33].

1.3 Motivation for a Numerical Study in Heterogeneous DWI

Ideally, we would like to gain insight into information of the microstructures of a heterogeneous cellular medium without making any hypothesis about the shape of the displacement probability density function. However, removing the assumption from DWI that diffusion follows a Gaussian can be very difficult. In fact, to replace the Gaussian with a function with a different shape, first, we would need to understand how the cellular microstructures affect the shape of the DPDF. In fact, predicting the shapes of the displacement densities in the presence of water restriction, such as in the case where particles encounter semi-permeable barriers, can be very challenging.

In order to address these questions, in this thesis, we develop two idealized models for tissues that are hoped to capture the diffusion of water molecules in a inhomogeneous medium. The idealized medium is made inhomogeneous by the presence of semi-permeable barriers that separate cellular and extracellular regions. We present a PDE model describing diffusion in the idealized medium and calculate the shape of the probability density functions for various sizes and configurations of the domain of computation. Having numerically computed the solutions, we can make some additional measurements of the moments of the probability density function and seek information about the structure of the medium as in an inverse problem.

The main advantage of the model used in this thesis is that it is versatile as all the parameters defining the geometry and the physiological properties can be adjusted to represent various structures without the need of complicated grids or numerical

methods. Such versatility would be not possible using an MRI machine directly. The important point of this work is that the mathematical approach applied, and the results obtained from the simulations, could be used to confirm DWI findings and to address specific questions that could not be answered in a conventional DWI experiment.

1.4 Thesis Outline

In Chapter 2 we describe the mathematical model for diffusion in cellular media starting with a brief description of human cells and tissues. Next we distinguish between homogenous, isotropic and anisotropic diffusion in cellular media. The last part of this chapter is dedicated to deriving an analytical expression for the DPDF for a diffusion process with particular attention to the cases of homogenous and non-homogenous diffusion.

Chapter 3 is entirely dedicated to Diffusion Weighted Imaging theory: we explain how a DW-MRI image is produced in practice and we define a mathematical expression to measure the signal of the experiment. In the last part of this chapter we introduce the fundamental concept of Apparent Diffusion Coefficient (ADC) and we derive ways for computing it.

Chapter 4 covers the core of this thesis. We present our idealized tissue models as well as the governing equations to describe diffusion in an inhomogeneous medium. We explain how to discretize the PDE model and we look at the structure of the matrix of the discretization. In the last section of this chapter, we reconsider the notion of ADC and present a new practical way of computing it for our model.

In Chapter 5, we establish the choice of computational and physiological parameters used to solve the PDEs numerically and present the results starting from some preliminary tests of the code. We present the numerical solution of the PDE for a simple problem and we look at the reliability and numerical accuracy of the solution. Next we present the solution for a more complex problem that simulates diffusion in an idealized inhomogeneous tissue. The last part of the chapter is dedicated to the measurements of the ADC using different definitions presented in Chapters 3 and 4. Finally, in Chapter 6 we summarize the benefits and potentials of our project for

DW-MRI experiments and point to some possible future work developments.

Chapter 2
Mathematical Models of Diffusion

Diffusion is a process that plays a fundamental role in the function of living organisms. Many biological systems rely strongly on the diffusion properties of cellular membranes [28]. It is possible that information about cellular structures can be obtained by studying the diffusion properties of water molecules as they cross the semi-permeable cellular membranes. To infer this information, diffusion MRI imaging techniques are used to track the diffusion of water molecules, because water is the most abundant constituent of most biological systems. In this process, simplified models for the displacement density (i.e., the Gaussian function) are often used. A better understanding of the effects of the inhomogeneities induced by the cellular structures may enable an analysis of the error caused by the simplifying assumption and show how the relaxation of the assumption can lead to the ability to extract more information from the imaging process.

In this chapter we will first give a brief insight into the complexity of the human cells and tissue structures. With regards to the complicated anatomy, we will then explain the characteristics of molecular diffusion in cellular media by giving some realistic examples of diffusion in a highly heterogenous medium and by highlighting the differences between free and restricted diffusion in cellular media. In the last section of this chapter we derive the mathematical form of the displacement probability density function by searching for the Green's function of the diffusion equation solved for a homogenous and inhomogeneous medium.

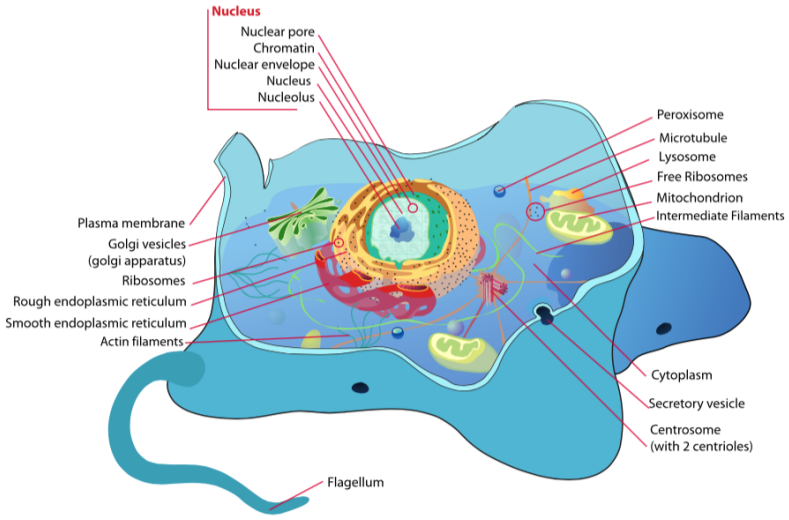

Figure 2.1: Diagram of a cell.
Source by: https://en.wikipedia.org/wiki/Cell_(biology)

2.1 Human Cell Anatomy

The human body is an extremely complex system. The structural, functional, and biological unit of the human body is the cell. Clusters of cells with the same origin and the same function constitute tissues. A collection of tissues joined in a structural unit to serve a common function is called an organ. Because each organ system is dedicated to a different function, each corresponding cell is unique not only in its function, but also in size, shape, and composition.

Human cells are enclosed in a protective cell membrane (see Figure 2.1). The cell membrane, surrounds the cytoplasm of a cell. This membrane serves to separate and protect a cell from its surrounding environment. The cell membrane is made of a double layer of phospholipids and a variety of protein molecules that act as channels and pumps that move different molecules into and out of the cell [10]. For this reason, the membrane is said to be semi-permeable. The cell membrane, in fact, can either let molecules of different type pass through freely, pass through to a limited extent, or not pass through at all. One of the main features of the cells in the human body is compartmentalization, that is, the presence of membrane-bound organelles (compartments) in which specific metabolic activities take place. Examples of such organelles

include mitochondria, the endoplasmic reticulum, the centrosome, vacuoles, ribosomes and the nucleus (see Figure 2.1). The molecular composition of cells includes mainly water (70%), simple and complex carbohydrates, fats and nucleic acids such as DNA and RNA [10] .

Cells are separated by extracellular space: this is defined as the tissue component outside the cells proper, thus outside the cell membranes, and occupied by fluid. The composition of fluid in the extracellular space includes, for the most part, water, as well as other chemical compounds such as metabolites, ions, various proteins and non-protein substances.

This complex structure makes the diffusion in cellular media a difficult process to describe. In the next section, we will develop a model for cellular diffusion in the presence of semi-permeable barriers.

2.2 Molecular Diffusion in Cellular Media

We use the term molecular diffusion to refer to the notion that any type of molecule in a fluid is randomly displaced as it is agitated by thermal energy. This process leads to ceaseless, irregular and apparently random motion of molecules in the medium [14]. The first reported experimental observations of a random walk of particles was made in 1828 by the botanist Robert Brown [16]. Brown noticed that particles of pollen, in water, were in an uninterrupted and irregular swarming motion. "Brownian motion"was described formally for the first time by Albert Einstein in 1905 [14][11]. Einstein understood that Brownian motion concerns the behaviour of a colloidal particle in a liquid and results from *random* molecular collisions with liquid molecules, leading to a motion, which can be described in terms of the random walk.

To clarify what we mean by random walk, let a particle start at the origin of the $x-$axis and execute N independent random steps of equal length Δx to the left or to the right. Let X_i be a random variable that assumes the value of δ if the particles moves to the right and $-\delta$ if it moves to the left. Let q be the probability that the particle moves to the left and $(1-q)$ the probability that it moves to the right. When the particle is crossing a cell membrane, we can assign a certain probability of it passing

though the membrane as the membranes microstructure may or may not allow it to pass.

Random diffusion is a non-deterministic process, which invariably leads to disorder in a system. Although random diffusion over time may contribute to the creation of essential reaction pathways in living matter, it is too disordered and disorganized to be relied on in life processes. Therefore, over evolutionary time, cells developed strategies to compartmentalize their anatomy using soft interfaces, fibres and scaffolding structures. Within these structures, macromolecules and sub-cellular entities undergo random and free diffusion. The typical length scales of these structures are in the range of $1 - 1000$ nm. This is the typical length scale where diffusional processes can be effective on the time scales that are relevant in biology [11]. The structuring and compartmentalization imply that the various diffusional processes take place in a highly heterogeneous medium. Therefore, the assumption of homogeneous and isotropic diffusion are poor.

In the following section, we will explain, using realistic examples, why diffusion in cellular media cannot be assumed to be isotropic by underlying some features which makes the medium inhomogeneous. Next, we will describe the processes of free and restricted water diffusion highlighting how the presence of obstacles can affect the diffusion of water molecules.

2.2.1 Example of direction-dependent diffusion in brain tissue

As explained in Section 2.1, the differences in cellular and extracellular structures, composition and organelle orientation can lead to significant changes in the shape of the displacement density of diffusing water molecules (see Section 1.2.1). For example, in the ventricles of the nervous system or other regions of the body that are mostly fluid-filled, there are relatively few microstructure barriers to diffusion. As such, particle displacements are equally likely in any direction and hence the diffusion is predominantly isotropic [2]. In other regions of the brain, such as in grey matter, there are several barriers to water mobility. In this case, where membrane structures are not aligned in any particular direction, the diffusion process remains isotropic as

well.

In white matter, neuronal axons are oriented parallel to each other with a greater consistency than that of cell walls in grey matter. Since displacements parallel to the fibre axis are, on average, larger than in directions perpendicular to the fibre axis, the diffusion in these tissues is anisotropic [2].

These various configurations of water diffusion in brain tissue can be applied to different types of tissue in various parts of the human body. Next, we will briefly discuss a model of diffusion in cellular media that can be applied to different types of tissue configurations and parameters.

2.2.2 Free and restricted diffusion in complex cellular media

We will use an example to illustrate the diffusion process in cellular media. We can imagine that at time $t = 0$, a given number N of labelled water molecules is free to move, from a starting point $x_0 = 0$, only along one dimension in a glass of water. The glass is assumed to be large enough so that it can be considered infinite. We are interested in measuring the displacement Δx after a specific time which we call the diffusion time interval Δt. If we count the number of molecules that travelled a certain distance $x_0 + \Delta x$, we see that most of the molecules travel short distances, and only a few travel farther. In fact, if we count the relative number n/N of particles that have travelled a certain distance, and we plot this information versus the displacement Δx, we observe that the histogram resembles a Gaussian distribution (see Figure 2.2). This is not surprising because the Gaussian distribution is the Green's function, also called *fundamental solution*, in the case of free diffusion in homogeneous media [32]. The exact shape of this distribution depends on different factors such as the type of molecule, temperature of the system and the diffusion time Δt. Depending on these variables, the distribution is going to be wider or narrower. Assuming that we are measuring the displacement in just one direction, the spread of the Gaussian over time is described by a single parameter: the variance $\sigma^2 = 2D\Delta t$, where D is the diffusion coefficient, which describes how easily the molecules are displaced. It follows that, for longer diffusion time Δt, we would expect a wider distribution as the particles

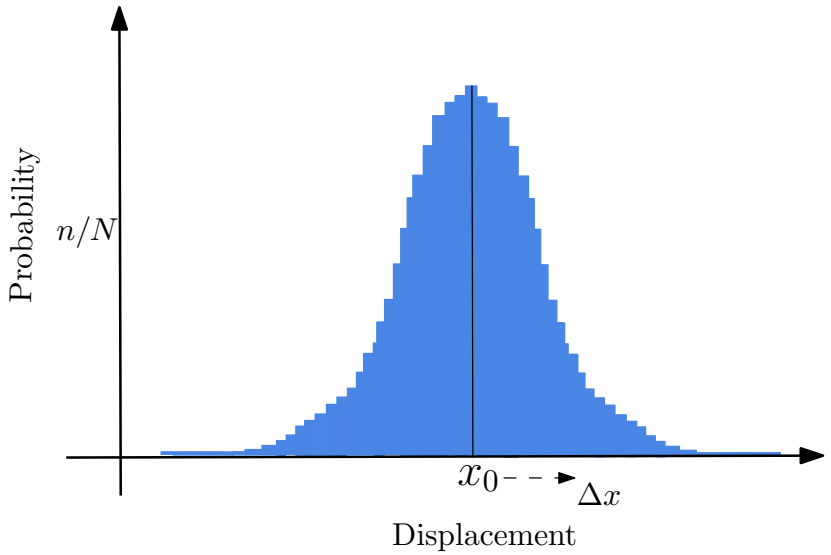

Figure 2.2: The histogram shows the typical displacement distribution due to diffusion in a one-dimensional model. For a source that starts at x_0, in a given diffusion time Δ, we can observe that only a few particles have travelled a long distance.

experience a longer displacement.

Consider now the same one-dimensional system with impermeable barriers distributed throughout at fixed locations. The displacement distribution associated within a volume element that contains one of the barriers and some of the surrounding liquid would be now significantly different than the one describing the free diffusion process. The difference reflects the presence of some restriction to diffusion in the system [14]. It is not easy to predict the shape of the Displacement PDF in this specific case, but, for sufficiently long diffusion times, it would be more or less bell-like and narrower than the one corresponding to free diffusion.

However, to better approximate a biological system, we can instead introduce semi-permeable interfaces that water molecules can cross with some resistance [14]. Over very short time scales, relatively few particles encounter the barriers and the diffusion would effectively be the same as in the case of free diffusion. As the time of observation increases, more particles encounter the barriers and eventually are transmitted or reflected. Therefore, the total displacement is less than it would have been without barriers.

Having introduced a model for the cellular diffusion, next, we will define the diffu-

sion tensor and discuss how its form changes in the case of homogeneous, isotropic or anisotropic diffusion.

2.2.3 The diffusion tensor

It is well known that, in the reaction-free case, any diffusion-like process can be modelled using the partial differential equation (PDE)

$$\frac{\partial \rho(\mathbf{r},t)}{\partial t} = -\nabla \cdot (D(\mathbf{r})\nabla \rho(\mathbf{r},t)). \tag{2.2.1}$$

In (2.2.1), $\rho(\mathbf{r},t)$ is the density of the particles and it depends both on the spatial position $\mathbf{r}$ and on the time t. $D(\mathbf{r})$ is called the diffusion tensor, and it is a symmetric positive definite rank-2 tensor field [23]. When we are measuring diffusion in more than one dimension, $D(\mathbf{r})$ is interpreted as a tensor because the relationship between the properties of the driving forces that generate diffusion and the resulting complex pattern of their movement in the tissue depends on the direction of the diffusion. Therefore, the collection of molecular displacements of this physical property can be described with nine components-each one associated with a pair of axes $xx, yy, zz, xy, yx, xz, zx, yz, zy$[26]. Because of the space dependence $D(\mathbf{r})$ is defined as a two dimensional (rank-2) tensor field. The $D(\mathbf{r})$ tensor is positive definite because its eigenvalues represent molecular mobility along the principal axes [20]. Finally, because $x \to y$ and $y \to x$ diffusivities should be the same, mirror-image off-diagonal elements are equal. This means the diffusion tensor matrix is symmetric with only 6 unique elements. The diffusion tensor can be written as

$$D(\mathbf{r}) = \begin{bmatrix} D_{xx} & D_{xy} & D_{xz} \\ D_{yx} & D_{yy} & D_{yz} \\ D_{xz} & D_{zy} & D_{zz} \end{bmatrix}. \tag{2.2.2}$$

If the material in which we are measuring the diffusion is homogenous (i.e., the diffusion is independent of position, and it is symmetric under translation [23]), then the diffusion tensor is constant (its entries are spatially independent). In the case where

we have isotropic diffusion, the diffusion tensor is proportional to the identity:

$$D(\mathbf{r}) = cI, \tag{2.2.3}$$

where I is the identity matrix and c is some constant coefficient. It is obvious that, for this case, the tensor $D(\mathbf{r})$ is diagonal. For this case, we have no preferred direction for diffusion and $D_{xx} = D_{yy} = D_{zz}$. In the case of anisotropic diffusion, (2.2.3) does not hold. The diffusion tensor is still symmetric and positive definite, but its entries off the main diagonal are not necessarily zero anymore. When we consider diffusion in just one dimension, there is no distinction between isotropy or anisotropy. In this case, the diagonal components of the diffusion tensor are equal, ($D_{xx} = D_{yy} = D_{zz}$), the diffusion tensor reduces to a scalar, and it is the diffusion coefficient D [6]. In the one dimensional case, (2.2.1) becomes

$$\frac{\partial \rho(x,t)}{\partial t} = -D(x)\frac{\partial^2 \rho(x,t)}{\partial x^2}. \tag{2.2.4}$$

Now that we have introduced the diffusion tensor and we have seen how it depends on the structure of the medium, we will go back to the density $\rho(\mathbf{r}, t)$ in the diffusion equation and will justify, mathematically, why it can be interpreted as a Displacement Probability Density Function.

2.3 The Displacement Probability Density Function

As explained in Section 1.2.1, the molecular diffusion process and the global behaviour of the molecules can be described using a Displacement Probability Density Function (DPDF). To relate the DPDF to a diffusion process, we must first relate the concept of a random walk to the Brownian motion. Given this result we introduce the probability density function for molecules experiencing random motion and relate it to the diffusion equation.

In Section 2.2 we defined the Brownian motion as a ceaseless and irregular random motion of particles colliding with fluid molecules. In the limit where the displacement that a particle experiences at each step goes to zero ($\Delta x \to 0$) and the number of collisions it undergoes is infinite ($N \to \infty$), then we can define $\rho(x, t)$ to be the

probability that at the time t the particle is located at the point x [35]. The probability density $\rho(x,t)$ satisfies the difference equation

$$\rho(x,t+\Delta t) = p\rho(x-\Delta x,t) + q\rho(x+\Delta x,t). \tag{2.3.1}$$

Equation (2.3.1) states that *the probability that the particle is at x at time $t+\Delta t$ equals the probability that it was at point $x-\Delta x$ at the time t multiplied by the probability p that it moved to the right in the following step plus the the probability that it was at point $x+\Delta x$ at the time t multiplied by the probability q that it moved to the left in the following step* [35].

Expanding in Taylor series with remainder $\rho(x,t+\Delta t)$ and $\rho(x\pm\Delta x,t)$ in(2.3.1) gives

$$\begin{cases} \rho(x,t+\Delta t) = \rho(x,t) + \Delta t\rho_t(x,t) + O(\Delta t^2), & \text{for the LHS} \\ \rho(x\pm\Delta x,t) = \rho(x,t) \pm \Delta x\rho_x(x,t) + \frac{1}{2}\Delta x^2\rho_{xx}(x,t) + O(\Delta x^3), & \text{for the RHS} \end{cases} \tag{2.3.2}$$

Substituting (2.3.2) into (2.3.1) we obtain

$$\frac{\partial\rho(x,t)}{\partial t} = (q-p)\frac{\Delta x}{\Delta t}\frac{\partial\rho(x,t)}{\partial x} + \frac{1}{2}(p+q)\frac{\Delta x^2}{\Delta t}\frac{\partial^2\rho(x,t)}{\partial x^2} + \mathcal{O}\left(\Delta t + \frac{\Delta x^4}{\Delta t}\right) \tag{2.3.3}$$

At this point, we shall assume that $p+q=1$ and that $p=q=1/2$. Making use of these assumption, and ignoring the higher order terms in the expansion, we can rewrite (2.3.3) as

$$\frac{\partial\rho(x,t)}{\partial t} = \frac{1}{2}\frac{\Delta x^2}{\Delta t}\frac{\partial^2\rho(x,t)}{\partial x^2} \tag{2.3.4}$$

From its definition [35], the expected value of the random variable X in this case is $\mathbb{E}(X) = (p-q)\Delta x n$, where n is the total number of particle we are considering. Having computed the expected value, we can write the variance of X as $\mathbb{V}(X) = 4pq\Delta x^2 n = D$. Making use of these definitions with $n = 1/\Delta t$, in the limit as $\Delta x \to 0$ and $\Delta t \to 0$, (2.3.4) tends to the partial differential equation

$$\frac{\partial\rho}{\partial t} = D\frac{\partial^2\rho}{\partial x^2} \tag{2.3.5}$$

where D is the called diffusion coefficient. Now, we can interpret ρ as a probability density associated with the continuous variable x at time t. In the next sections we

will derive a mathematical expression for the DPDF in the case of diffusion occurring in an homogeneous or inhomogeneous medium.

2.3.1 DPDF for an homogenous medium

As explained is Section 1.2.1, if we consider diffusion in a homogenous medium, we expect the probability density function to have a Gaussian profile. It is important to make clear that having an unbounded domain is necessary when considering a homogeneous medium. In this section, we want to show this by deriving the expression for the Green's function for the 1D diffusion equation defined over the infinite domain, $-\infty < x < +\infty$. More precisely, we want to find a form for the Green's function [35] $K(x,t;\xi,\tau)$ such that it is a solution to the problem

$$\frac{\partial K(x,t;\xi,\tau)}{\partial t} - D\frac{\partial^2 K(x,t;\xi,\tau)}{\partial x^2} = -\delta(x-\xi)\delta(t-\tau), \quad \infty < x < +\infty; \quad t,\tau < \Delta, \tag{2.3.6}$$

and satisfies the initial condition $K(x,t,\xi,\tau) = 0$ where (ξ,τ) is some specific space-time point in our domain. In (2.3.6), the functions on the RHS are Dirac delta functions in space and time.

In order to solve the IVP for the Green's function, we use the Fourier transform in the spatial variable x. Denoting the Fourier transform of $K(x,t;\delta,\tau)$ as $k(\lambda,t;\delta,\tau)$ we can write, from the definition of Fourier transform [35],

$$k(\lambda,t;\delta,\tau) = \frac{1}{\sqrt{2\pi}}\int_{-\infty}^{\infty} e^{-i\lambda x}K(x,t;\delta,\tau)dx. \tag{2.3.7}$$

Multiplying (2.3.6) by $(1/\sqrt{2\pi})e^{-i\lambda x}$, integrating with respect to x on the whole domain and using the differentiation property for the Fourier transform

$$\frac{1}{\sqrt{2\pi}}\int_{-\infty}^{+\infty} e^{-i\lambda x}f^{(n)}(x)dx = (-i\lambda)^n F(\Lambda), \tag{2.3.8}$$

we obtain an equation for $k(\lambda,t;\delta,\tau)$

$$\frac{\partial k(\lambda,t;\xi,\tau)}{\partial t} - (D\lambda)^2 k(\lambda,t;\xi,\tau) = \frac{-1}{\sqrt{2\pi}}e^{-i\lambda\xi}\delta(t-\tau). \tag{2.3.9}$$

Using an integrating factor, the solution of the first-order differential equation (2.3.9)

is

$$k(\lambda, t; \xi, \tau) = \frac{1}{\sqrt{2\pi}} \exp[(D\lambda)^2(\tau - t) - i\lambda\xi]H(t - \tau), \tag{2.3.10}$$

where $H(t-\tau)$ represents the Heaviside step function centered at $t = \tau$. The inverse Fourier transform of $K(x, t; \delta, \tau)$ in (2.3.10) is

$$K(x, t; \xi, \tau) = \frac{1}{2\pi} H(\tau - t) \int_{-\infty}^{\infty} \exp[i\lambda(x - \xi) - D\lambda^2(\tau - t)]d\lambda. \tag{2.3.11}$$

Evaluating the integral, we find the Green's function for the diffusion equation

$$K(x, t; \xi, \tau) = \frac{H(\tau - t)}{\sqrt{(4\pi D^2(\tau - t))}} \exp\left[-\frac{(x - \xi)^2}{4D^2(\tau - t)}\right]. \tag{2.3.12}$$

The obtained Green's function $K(x, t; \xi, \tau)$ can be used to find a solution $\rho(x, t)$ for the diffusion equation

$$\frac{\partial \rho}{\partial t} - D\frac{\partial^2 \rho}{\partial x^2} = F(x, t) \qquad -\infty < x < \infty; t > 0 \tag{2.3.13}$$

when the initial condition is: $\rho(x, 0) = \delta(x - \xi)$. The solution formula is

$$\rho(\xi, \tau) = \int_0^{\Delta} \int_{-\infty}^{\infty} K(x, t; \xi, \tau)F(x, t)dxdt + \int_{-\infty}^{\infty} K(x, 0; \xi, \tau)\delta(x - \xi)dx. \tag{2.3.14}$$

In our case, the first integral vanishes because $F(x, t)$ is zero. Moreover, because $H(\tau - t) = 0$ for $t > \tau$, the second integral becomes

$$\int_{-\infty}^{\infty} K(x, t; \xi, \tau)\delta(x - \xi)dx = \frac{1}{2\sqrt{D\pi\tau}} \int_{-\infty}^{\infty} e^{(x-\xi)^2/4D\tau}\delta(x - \xi)dx. \tag{2.3.15}$$

Therefore, we can conclude that the solution to the 1D diffusion equation, when the initial condition is a Dirac delta function, is

$$\rho(x, t) = \frac{1}{2\sqrt{D\pi t}} \int_{-\infty}^{\infty} e^{(x-\xi)^2/4Dt}\delta(x - \xi)dx. \tag{2.3.16}$$

That is, the source function is

$$S(x, t) = \frac{1}{2\sqrt{\pi Dt}} e^{(x-\xi)^2/4Dt}, \qquad \text{for } t > 0. \tag{2.3.17}$$

This result justifies the interpretation of the function $\rho(x, t)$ as a DPDF for molecules diffusing in an homogenous medium. A physical interpretation for our purposes of (2.3.16) is the following: *Suppose we are observing Brownian motion where particles are moving in one dimension. Then the probability that a particle that begins at position* ξ *ends up in the interval* (a, b) *at time* t *is precisely* $\int_a^b S(x - \xi, t)d\xi$ *where* S *is the*

source function for the diffusion equation [32].

2.3.2 DPDF for an inhomogenous medium

If we do not consider an infinite domain in our problem, then the Green's function for the diffusion function is no longer a Gaussian. This is due to the fact that limiting the domain to a bounded region, as well as introducing membranes in the model, affect the form of the Green's function rendering it much more complex. This point is very important for the purpose of this work: in fact, as we will explain (see Section 4.1), our domain is not infinite and the presence of semi-permeable barriers is modelled by boundary conditions at each of these interfaces.

To derive the Green's function for the one-dimensional parabolic equation in a bounded region, we start by considering the general boundary value problem (BVP)

$$\nu(x)\frac{\partial\rho(x,t)}{\partial t} - \frac{\partial}{\partial x}\left(p(x)\frac{\partial\rho(x,t)}{\partial x}\right) + q(x)\rho(x,t) = \nu(x)F(x,t), \qquad 0 < x < l, t > 0, \tag{2.3.18}$$

with initial condition

$$\rho(x,0) = f(x), \tag{2.3.19}$$

and boundary condition

$$\alpha_1\rho(0,t) - \beta_1\rho_x(0,t) = g_1(t) \qquad \alpha_2\rho(l,t) - \beta_2\rho_x(l,t) = g_2(t). \tag{2.3.20}$$

Equation (2.3.18) is the most generic example of one-dimensional parabolic PDE, where $\nu(x)$, $p(x)$, $q(x)$ and $F(x,t)$ are linear generic terms depending on the space variable x and on time t. The domain of integration is assumed to be a bounded region ($0 < x < l$), and the time is assumed to be positive ($t > 0$). This derivation is valid for any spatially dependent initial condition of the form (2.3.19). The conditions at the boundaries, as specified in (2.3.20), may be Dirichlet, Neumann or mixed boundary condition. In order to write an integral relation to find the solution at the generic point $\rho(\xi,\tau)$ for the BVP, we can define [35], a one-dimensional space-time gradient operator $\tilde{\nabla} = [\partial/\partial x, \partial/\partial t]$ and a one-dimensional differential operator L such that

$$L\rho(x,t) = -\frac{\partial}{\partial x}\left(p(x)\frac{\partial\rho(x,t)}{\partial x}\right) + q(x)u. \tag{2.3.21}$$

With the use of the operator L, we can rewrite (2.3.18) as

$$\nu(x)\frac{\partial \rho(x,t)}{\partial t} + L\rho(x,t) = \nu(x)F(x,t). \tag{2.3.22}$$

Applying the operator $\tilde{\nabla}$ to (2.3.22), and using the fundamental theorem of calculus, we can obtain the following integral relation [35]

$$\begin{aligned}
&\int_0^T \int_0^l [K(\nu\rho_t + L\rho) - \rho(-\nu K_t + LK)]dxdt \\
&= -\int_0^l [\nu K\rho]|_{t=0}dx + \int_0^T [-\nu K\rho_x + \nu\rho K_x]|_{x=l}dt \\
&+ \int_0^l [\nu K\rho]_{t=T}dx - \int_0^T [\nu K\rho_x + \nu\rho K_x]|_{x=0}dt,
\end{aligned} \tag{2.3.23}$$

where the subscript x or t denotes the derivatives with respect to space and time respectively and $K(x,t;\xi,\tau)$ is the generic Green's function. If the space-time point (ζ,τ) is inside our domain of integration, then we can choose the function $K(x,t;\xi,\tau)$ to be a solution of the parabolic problem

$$-\nu(x)K_t(x,t;\xi,\tau) + LK(x,t;\xi,\tau) = \delta(x-\xi)\delta(t-\tau) \qquad \xi < l; t,\tau < T. \tag{2.3.24}$$

If $\alpha_1 = \alpha_2 = 0$ in (2.3.20), then we have Neumann boundary conditions and we can rewrite the second and fourth integral in the RHS of (2.3.23) as

$$\int_0^T [-\nu K\rho_x + \nu\rho K_x]|_{x=l}dt = \int_0^T \frac{\nu(l)}{\beta_2} g_2(t)K_x(l,t;\xi,\tau)dt, \tag{2.3.25}$$

and

$$\int_0^T [\nu K\rho_x + \nu\rho K_x]|_{x=0}dt = \int_0^T \frac{\nu(l)}{\beta_1} g_1(t)K_x(0,t;\xi,\tau)dt, \tag{2.3.26}$$

respectively. Combining the results in (2.3.23), (2.3.25) and (2.3.26), the solution formula for the arbitrary point $\rho(\xi,\tau)$ in the one-dimensional parabolic case is given by

$$\begin{aligned}
\rho(\xi,\tau) = &\int_0^T \int_0^l \nu(x)F(x,t)K(x,t;\xi,\tau)dxdt + \int_0^l \nu(x)f(x)K(x,0;\xi,\tau) \\
&+ \int_0^T \left[\frac{\nu(l)}{\beta_2} g_2(t)K_x(l,t;\xi,\tau) - \frac{\nu(l)}{\beta_1} g_1(t)K_x(0,t;\xi,\tau)\right] dt.
\end{aligned} \tag{2.3.27}$$

If the RHS of (2.3.18) is equal to 0, then the first integral in (2.3.27) vanishes, and, in the case of constant Neumann boundary conditions so does the third integral in the same equation.

Next, we want to find an expression for the Green's function $K(x,t;\xi,\tau)$ in the inhomogeneous case. In order to do that, we expand $K(x,t;\xi,\tau)$ in a series of eigenfunctions: $K(x,t;\xi,\tau) = \sum_{k=1}^{\infty} N_k(t)M_k(x)$. Here $M_k(x)$ are the eigenfunctions of the operator L that satisfy the BVP. Multiplying (2.3.24) by $M_k(x)$ and integrating over the domain, we obtain

$$-N_k^{'}(t) + \lambda_k N_k(t) = M_k(\xi)\delta(t-\tau), \qquad t,\tau < T; k = 1,2\ldots \tag{2.3.28}$$

Using the fact that $\delta(t-\tau) = \delta(\tau - t)$, we can rewrite (2.3.28) as

$$-\frac{d}{dt}[e^{-\lambda_k t}N_k(t)] = M_k(\xi)e^{-\lambda_k t}\delta(t-\tau) = M_k(\xi)e^{-\lambda_k \tau}\delta(\tau - t), \tag{2.3.29}$$

where the symmetry property of the Dirac delta has been used. Integrating (2.3.29), and using $N_k(0) = 0$ as the initial condition, we get

$$N_k(t) = e^{-\lambda_k(t-\tau)}M_k(\xi)H(\tau - t), \tag{2.3.30}$$

where $H(t)$ denotes the Heaviside step function. Finally, recalling that $dH(x)/dx = \delta(x)$, the Green's function can be written as

$$K(x,t;\xi,\tau) = \left[\sum_{k=1}^{\infty} e^{-\lambda_k(t-\tau)}M_k(\xi)M_k(x)\right] H(\tau - t). \tag{2.3.31}$$

Both the results that have been shown in this section (equations (2.3.27) and (2.3.31)) demonstrate that a simple extension such as bounding the domain, can result in a significant complication of the form of the solution for a single point and of the Green's function (and consequently the form of the Source Function). We conclude then, that without the assumption of homogeneity, the Probability Density Function cannot be considered to have a Gaussian form. In fact, it is easy to see that substituting (2.3.31) into (2.3.27) we do not get a Source function that is a Gaussian.

Chapter 3
Diffusion Weighted Imaging

Diffusion Weighted Imaging (DWI) is the simplest of a variety of diffusion MRI techniques (see Section 1.2). In particular, DWI is an inherently one-dimensional MR-imaging technique that makes MRI sensitive to the process of water molecular diffusion, yielding micro-structural insights into the states of tissues. Free molecules, such as water, are in constant random motion due to the thermal energy associated with their body temperature. As discussed in Section 2.2, this random motion suggests that, over time, a molecule will undergo a certain displacement in a random direction. Information regarding the average magnitude of the random displacement can be inferred by a quantity known the *Apparent Diffusion Coefficient* (ADC).

We will start this chapter by explaining how a Diffusion Weighted Image is created through the use of a specific spin-echo sequence in an MRI experiment. Next, we will introduce a mathematical way to express the signal and, from here, we will derive and justify various expressions for the Apparent Diffusion Coefficient.

3.1 Creating a Diffusion Weighted Image

3.1.1 Basic physics of MRI

To understand how a Diffusion Weighted Image is created, it is useful to give here some explanations about the basics of the MRI physics. The units of a biological sample are the atomic nuclei and their orbiting electrons. A fundamental property of nuclei with odd atomic weight and/or odd atomic number is that they posses an intrinsic angular momentum $\vec{J}$. An important property of a nuclear spin system, i.e., an ensemble

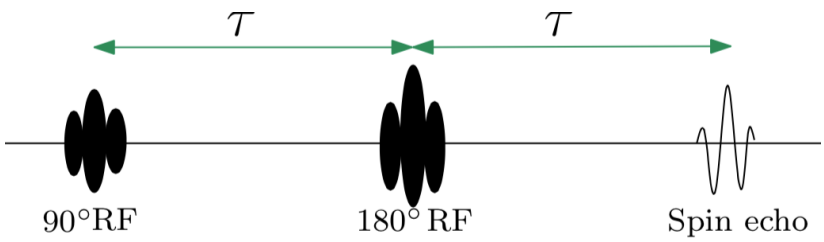

Figure 3.1: Standard Spin Echo sequence

of nuclei of the same type [34], is *nuclear magnetism*. As with any classical spinning charged objects, a nucleus with a nonzero angular momentum creates a magnetic field. The presence of this magnetic field is represented by the magnetic moment $\vec{\mu}$. Due to the thermal random motion, the direction of $\vec{\mu}$ is completely random and *no* magnetic field is observable in a macroscopic object. To line up the spin vectors, an external, static magnetic field $\vec{B_0}$ is applied. The macroscopic effect of the external field $\vec{B_0}$ is the generation of an observable bulk magnetization $\vec{M} = \sum_{n=1}^{N} \vec{\mu_n}$ pointing along the direction of $\vec{B_0}$. At the equilibrium, the transverse component of $\vec{M}$ is zero because the precessing magnetic moments have random phases. Establishments of a phase coherence is called *resonance* and it can be achieved by a sequence of RF pulses after which a signal (*echo*) can be measured.

The pulse sequence used to generate a DW image differs from the basic Spin-Echo sequence often used in MRI. The basic Spin-Echo sequence (see Figure 3.1) is generated using two RF pulses [34]. The first pulse is a 90° pulse which has the effect of rotating the nuclear spins into the transverse plane, and thus, they begin to precess about the z-axis, the direction of the main field B_0 (see Figure 3.4). Due to the relatively small local magnetic field inhomogeneities (variations in the magnetic field at different parts of the sample) the spins will have slightly different precessional frequencies. Thus, after some time they will lose phase coherence as the free precession continues (see Figure 3.2b) [8]. After a time $t = \tau$, the second pulse, (a 180° pulse), is applied. This pulse has the effect of flipping the spins over to the other side of the transverse plane (Figure 3.2c). Because all the spins will still precess at the same rate as before the second pulse, the faster will catch the slower and, at time $t = 2\tau$, the phase coherence

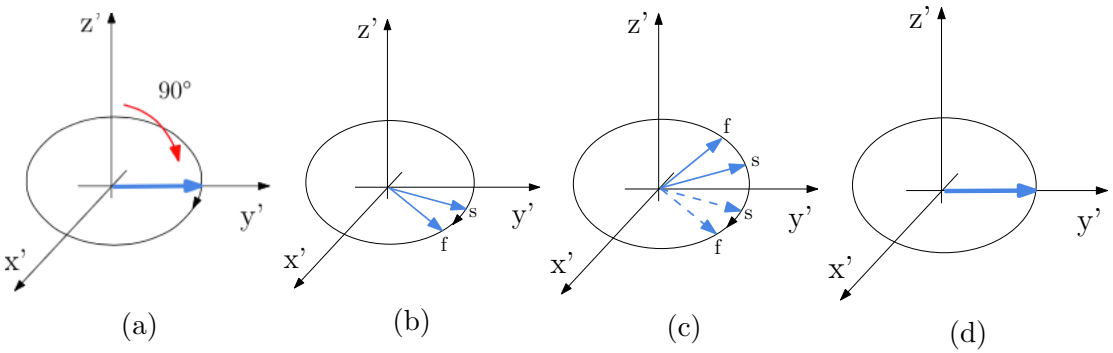

Figure 3.2: Vector diagram illustrating the refocusing of spins in a standard Spin Echo sequence. The letters f and s denote the faster and slower spins respectively. At the beginning the spins are in phase (a). Just after the 90° pulse is applied, since one is precessing faster than the other, they will start dephasing (b). At time $t = \tau$, the 180° pulse, about the y' axis, has the effect of flipping them (c) so that, at time $t = 2\tau$ the faster will catch the slower recreating phase coherence (d).

will be restored (Figure 3.2d). If the echo, i.e., the capturing of the signal, occurs at this time, the attenuation of the signal due to dephasing of the spins will be minimized.

The Spin-Echo sequence described above is unable to capture diffusion behaviours. However, an additional encoding procedure can turn the spin-echo sequence into a DW-MRI acquisition used to study the diffusion of water molecules [27]. In particular, two short, high-amplitude, magnetic field gradients are added after the 90° and 180° pulses transforming the spin-echo into a Diffusion Weighted (DW) spin-echo (see Figure 3.3). The effect of these gradient pulses is to accelerate spin precession of individual water molecules (see Figure 3.4) according to their spatial position. For example, if the gradient field is applied along the z direction, spins associated with water molecules with high z coordinates will precess more quickly whereas spins associated with water molecules at low z coordinates will precess more slowly. Overall, the ensemble of spins will precess at different rates and consequently *dephase*, where the magnitude of dephasing will depend on the relative position of the molecules. A 180° RF pulse, followed by a gradient pulse of equal amplitude and duration is then applied, which has the effect of flipping the spins allowing the rephasing at which point the echo is acquired.

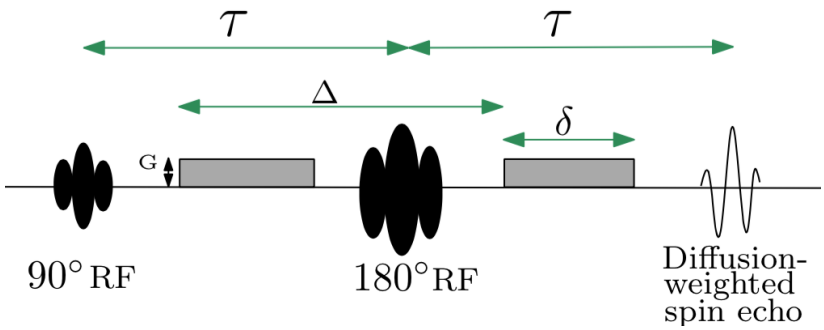

Figure 3.3: Diffusion Weighted Imaging Spin Echo sequence

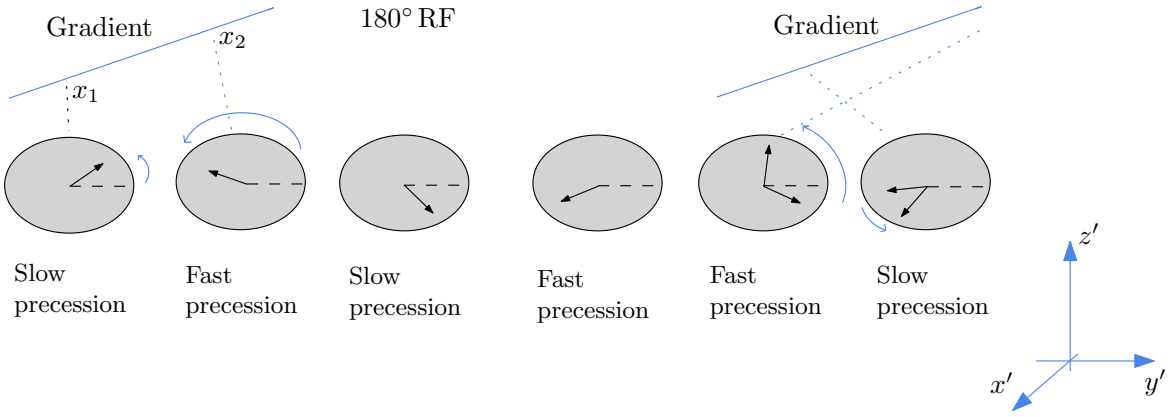

Figure 3.4: Representation of the dephasing of the different spin during the Spin Echo Pulse Sequence used in diffusion weighted imaging. If there is displacement of water molecules after the first gradient pulse and before the second, thus the position in the gradient field are not the same during the 90° and 180° pulse, there will be a net loss of spin echo amplitude.

If the individual spins are at exactly the same spatial coordinates during both gradient pulses, the phase refocusing will be theoretically exact and there will be no net loss of signal in the resultant spin-echo. However, if a molecule moves in between the two gradient pulses (see Figure 3.4), then a different amplitude of the gradient will be experienced during the second gradient and the phase refocusing will be incomplete and a loss of spin-echo amplitude will be experienced (see Figure 3.4). The larger the distance travelled, the larger the phase difference and the larger the signal loss will be. As such, the diffusion of molecules in the time between the two gradient pulses, called the diffusion time Δ, can be encoded in the spin-echo amplitude [30]. As we will see in the following section, tuning the amplitude and the length of the gradient pulses is fundamental in order to measure the diffusion of water.

3.1.2 Measuring the MRI signal for a DW image

In DW-MRI, there is a loss in the strength of the signal due to the diffusion of the water molecules. Mathematically, we can express this with a definition that correlates the signal attenuation to the distance travelled by the molecules [31] [30]

$$R(\Delta) = \frac{1}{L(\Omega)} \int_{\Omega^-}^{\Omega^+} \int_{\Omega^-}^{\Omega^+} \rho(x|x_0, \Delta) \cos[q(x - x_0)] dx dx_0, \tag{3.1.1}$$

where $\rho(x|x_0, \Delta)$ is the displacement PDF and $R(\Delta)$ is the measured signal. In (3.1.1), $\Omega \equiv [\Omega^-, \Omega^+]$ is the domain covering the sample and $L(\Omega)$ is the length of the sample. The function $\rho(x|x_0, \Delta)$ describes the probability that an hydrogen proton starting at position x_0 is at x after the diffusion time Δ (see Section 2.3). The factor $q = \gamma \delta G$, where γ is the gyromagnetic ratio, δ is the duration of the gradient pulse and G is the intensity (amplitude) of the gradient (see Figure 3.3). From this definition it follows that the units for q are [rad/μm], i.e., q gives the relation between phase and position. The cosine function in (3.1.1) describes the dephasing angle between molecules at the end of the DW- Spin-Echo sequence and it can be interpreted as an attenuating factor due to this dephasing.

In (3.1.1), $R(\Delta)$ is defined to be the *relative* echo height. In fact, it is the ratio of the signal measured when the value of q is not zero, $S(q \neq 0)$, and when the value of

q is zero, $S(q = 0)$. Therefore, we can say that the signal is normalized, i.e., $R = 1$ in the absence of the diffusion sensitization gradients (i.e., when $q = 0$) (see Figure 3.3). Assuming that the concentration of molecules is constant throughout the domain over the entire diffusion time, and that the domain of computation is a infinite periodic lattice with lattice constant α (i.e., the contribution from each lattice unit is the same), in order to assume homogeneity, we can write the expression for the normalized signal $R(\Delta)$ as

$$R(\Delta) = \frac{1}{\alpha} \int_0^{\alpha} \int_{\Omega^-}^{\Omega^+} \rho(x|x_0, \Delta) \cos[q(x - x_0)] dx dx_0, \tag{3.1.2}$$

where we just replaced the bounds of integration.

The term q is directly related to the gradient application [6], and it determines the magnitude of the attenuating effect of the proton dephasing due to the displacement of water molecules. Because q depends on the duration of the gradient pulses as well, the easiest way to change its value is to lengthen the duration of the two gradient pulses. In this way, the longer the duration, the less the water molecules will have to move to produce a similar signal loss [24]. The important point is that we can control the value of q by changing the intensity G and the duration δ of the gradient pulses. Depending on these changes we can expect a difference in the signal loss.

Having introduced and explained the mathematical expression for the signal in a DW-MRI experiment, we will now introduce the most widely used measure in diffusion weighted imaging: the Apparent Diffusion Coefficient (ADC).

3.2 The Apparent Diffusion Coefficient

A quantitative measure derived from a DWI experiment is the Apparent Diffusion Coefficient (ADC). The ADC is a measure of the freedom of water molecular diffusion in the tissue environment and encodes information about an average distance water molecules diffuse [17]. A numerical value of the ADC depends on interactions of the diffusing molecules of water with cellular and extracellular structures over a given time. It follows that a decrease in the ADC is interpreted as a reduced diffusion of water, whereas in tissue with an increased ADC, there is less restriction to the diffusion [17].

Even though more complex and sophisticated imaging techniques have been developed (see Section 1.2), DWI and measurements of the ADC are still effective when the orientation of the structures within the tissue is not important (i.e., isotropic medium). In these cases, it is sufficient to characterize the diffusion with a scalar ADC (see Section 2.2.3) [6]. In this thesis we focus on DWI and the ADC because the effects of inhomogeneities in an isotropic medium would be reflected in a similar way in an anisotropic medium.

In the next section, we will show how we can derive an expression for the ADC from the measured DW-Spin-Echo signal $R(t)$.

3.2.1 Measuring the ADC from the signal: a theoretical approach

In this section we will show that, even without prior knowledge of the internal structure of our system (i.e., without knowing the form of the DPDF $\rho(x,t)$), it is possible to compute a value for the apparent diffusion coefficient from a measured MRI signal $R(\Delta)$. We begin the derivation by considering an equation [1] used to describe a diffusion-spin-echo experiment for the case of a 90° pulse followed by a 180° pulse as shown in Figure 3.5 assuming homogeneity in the medium [30]

$$\frac{\partial \Psi}{\partial t} = -i\gamma(\mathbf{r}\cdot\mathbf{G})\Psi + D\nabla^2\Psi, \tag{3.2.1}$$

where Ψ is the net magnetization of nuclei in the transverse plane, $\mathbf{r}$ is the vector of coordinates, $\mathbf{G}$ is a constant magnetic field collinear with the B_0-field and D is the diffusion coefficient.

Consider the behaviour of the solution Ψ in the absence of the diffusion term

$$\frac{\partial \Psi}{\partial t} = -i\gamma(\mathbf{r}\cdot\mathbf{G})\Psi. \tag{3.2.2}$$

First, we solve for the solution Ψ for $0 \leq t \leq \tau$ (i.e., between the 90° and the 180° pulses). In this case, we can use an integrating factor to get

$$\Psi = S(t)e^{-i\gamma\mathbf{r}\cdot\mathbf{F}(t)}, \tag{3.2.3}$$

where *S(t)* represents the transverse magnetization at any point in time (i.e., the measurable signal) [19] and the integrating factor is $\mathbf{F}(t) = \int_0^t \mathbf{G}(t')dt'$. Now we

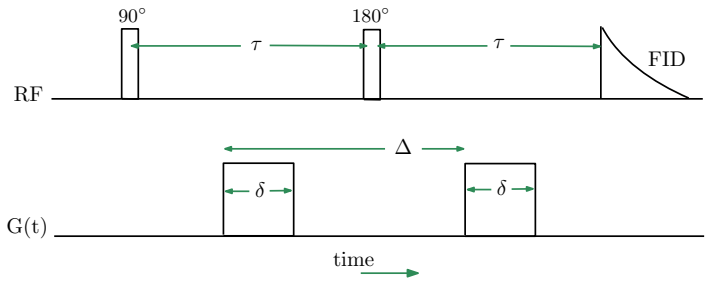

Figure 3.5: Pulse Gradient Spin Echo sequence. The RF pulse sequence consists of a 90° and a 180° pulse separated by the time τ, the Free Induction Decay is recorded after a time 2τ, at the peak of the spin echo. The magnetic field gradient pulses are of equal duration δ, and separated by the time interval Δ.

consider the solution Ψ for $t \geq \tau$ (i.e., after the 180° pulse). The effect of this pulse is to reduce the phase of Ψ by twice the amount which it has increased. Therefore, we can write the complete solution of (3.2.1) as

$$\Psi = S(t)e^{-i\gamma\mathbf{r}\cdot(\mathbf{F}(t)+(\beta-1)\mathbf{f})}. \tag{3.2.4}$$

The coefficient β is chosen so that the second exponent in (3.2.4) is 0 between the 90° and the 180° during which $\mathbf{F}(t)$ increases from $\mathbf{F}(0)$ to $\mathbf{F}(\tau)$. After the 180° pulse, the second exponent turns into $-2\mathbf{f}$ (constant), and the first part of the exponent continues to increase from $\mathbf{F}(\tau)$ to $\mathbf{F}(2\tau)$. A spin-echo occurs when $\mathbf{F}(2\tau) = -2\mathbf{f}(2\tau)$ and the exponential term equates to one [19]. Differentiating (3.2.4) with respect to time, we obtain

$$\frac{\partial\Psi}{\partial t} = \frac{dS(t)}{dt}e^{-i\gamma\mathbf{r}\cdot(\mathbf{F}(t)+(\beta-1)\mathbf{f})} - S(t)i\gamma\mathbf{r}\cdot\left(\frac{d\mathbf{F}(t)}{dt} + (\beta-1)\frac{d\mathbf{f}}{dt}\right)e^{-i\gamma\mathbf{r}\cdot(\mathbf{F}(t)+(\beta-1)\mathbf{f})}. \tag{3.2.5}$$

Now we include the diffusion term in (3.2.1). The solution is very similar to the previous case. Because $S(t)$ depends just on time and the Laplacian double derivative is taken with respect to the spatial vector $\mathbf{r}$ we can write

$$\begin{aligned}\Psi &= DS(t)\nabla^2 e^{-i\gamma\mathbf{r}\cdot(\mathbf{F}(t)+(\beta-1)\mathbf{f})},\\ &= DS(t)(-i\gamma\mathbf{r}\cdot(\mathbf{F}(t)+(\beta-1)\mathbf{f}))\nabla e^{-i\gamma\mathbf{r}\cdot(\mathbf{F}(t)+(\beta-1)\mathbf{f})},\\ &= DS(t)(\gamma\mathbf{r}\cdot(\mathbf{F}(t)+(\beta-1)\mathbf{f}))^2 e^{-i\gamma\mathbf{r}\cdot(\mathbf{F}(t)+(\beta-1)\mathbf{f})}.\end{aligned} \tag{3.2.6}$$

Substituting (3.2.6) into (3.2.1) we get

$$\frac{\partial \Psi}{\partial t} = -i\gamma \mathbf{G}\cdot\mathbf{r}\Psi - DS(t)(\gamma \mathbf{r}\cdot(\mathbf{F}(t)+(\beta-1)\mathbf{f}))^2 e^{-i\gamma \mathbf{r}\cdot(\mathbf{F}(t)+(\beta-1)\mathbf{f})}. \tag{3.2.7}$$

From now on, to simplify the notation, we will set $\Phi(t) = -i\gamma(\mathbf{F}(t)+(\beta-1)\mathbf{f})$ [30]. Next, we equate (3.2.5) and (3.2.7) and use (3.2.4) to get

$$\frac{dS(t)}{dt}e^{\Phi} - S(t)(-i\gamma \mathbf{r}\cdot\mathbf{G})e^{\Phi} = -S(t)(-i\gamma \mathbf{r}\cdot\mathbf{G}) - DS(t)(\gamma(\mathbf{F}(t)+(\beta-1)\mathbf{f}))^2 e^{\Phi}. \tag{3.2.8}$$

Algebraic simplification yields

$$\frac{dS(t)}{dt} = -DS(t)(\gamma(\mathbf{F}(t)+(\beta-1)\mathbf{f}))^2. \tag{3.2.9}$$

Now we can solve (3.2.9) by separation of variables:

$$\int_{S(0)}^{S(2\tau)} \frac{dS(t)}{S(t)} = -D\gamma^2 \int_0^{2\tau} (\mathbf{F}(t)+(\beta-1)\mathbf{f}))^2 dt. \tag{3.2.10}$$

The integral in the RHS of (3.2.10) is not easy to evaluate, but it can be shown (see [30]) that, in the case where the two gradient pulses are very short, the result is simply

$$\ln\left(\frac{S(2\tau)}{S(0)}\right) = -D\gamma^2 G^2 \delta^2 \Delta = -D\Delta q^2, \tag{3.2.11}$$

where Δ is the diffusion time and D is, in the case of a homogenous medium, the diffusion coefficient. The entire previous theoretical derivation is to show and to justify (3.2.11); this result is widely used in the literature. In practice, one would measure the signal with and without the sintetizing gradients, $(S(q \neq 0))$ and $(S(q = 0))$. Having chosen q and the diffusion time, one would calculate the Apparent Diffusion Coefficient directly from (3.2.11).

3.2.2 Calculating the ADC: a probabilistic approach

The result in (3.2.11) is often used in practice. However, it is instructive to consider an alternative derivation. If the medium is homogenous the diffusion coefficient can be found from the second moment of the displacement probability density function

$$D = \frac{1}{2\Delta L[\Omega]} \int_{\Omega^-}^{\Omega^+} \int_{\Omega^-}^{\Omega^+} \rho(x|x_0,\Delta)(x-x_0)^2 dx dx_0. \tag{3.2.12}$$

We recall the relation (3.1.1) between the DPDF ρ and the MRI relative signal $R(t)$, and replace the cosine function with its Maclaurin series expansion. By Taylor expanding the cosine in (3.1.1) with respect to $q(x-x_0)$ we get

$$\begin{aligned} R(\Delta) &= \frac{1}{L(\Omega)} \int_{\Omega^-}^{\Omega^+} \int_{\Omega^-}^{\Omega^+} \rho(x|x_0,\Delta)\cos[q(x-x_0)]dxdx_0, \\ &\sim \frac{1}{L(\Omega)} \int_{\Omega^-}^{\Omega^+} \int_{\Omega^-}^{\Omega^+} \rho(x|x_0,\Delta)\left[1 - q^2\frac{(x-x_0)^2}{2!} + \cdots\right]dxdx_0, \\ &= \frac{1}{L(\Omega)} \int_{\Omega^-}^{\Omega^+} \int_{\Omega^-}^{\Omega^+} \rho(x|x_0,\Delta)dxdx_0 - \\ &\quad - \frac{1}{L(\Omega)} \int_{\Omega^-}^{\Omega^+} \int_{\Omega^-}^{\Omega^+} \rho(x|x_0,\Delta)q^2\frac{(x-x_0)^2}{2!}dxdx_0 + \mathcal{O}(q^4(x-x_0)^4). \end{aligned} \tag{3.2.13}$$

If we assume that the domain of integration is big enough and that the sample is homogenous then the first term on the right-hand side of (3.2.13) is 1; by definition of the DPDF-being a probability density function, its integral over $\mathbb{R}$ is necessarily 1. The second term on the right-hand side of (3.2.13), up to a scaling factor, assuming homogeneity, is the diffusion coefficient D as given in (3.2.12); as such, the second term in (3.2.13) can be written as $q^2\Delta D$. Therefore, if we neglect the $\mathcal{O}(q^4(x-x_0)^4)$ terms, then, given a homogenous medium, the diffusion coefficient can be computed via:

$$R(\Delta) = 1 - q^2\Delta D. \tag{3.2.14}$$

However, because of the presence of inhomogeneities in the medium, the value of the diffusion coefficient changes in time. Therefore, we can define the apparent diffusion coefficient by writing (3.2.14) as

$$R(\Delta) = 1 - q^2\Delta D^{(2)}_{\text{ADC}}(\Delta), \tag{3.2.15}$$

where the superscript 2 denotes the ADC computed from a second-order Taylor expansion. Taking the natural logarithm of both sides of (3.2.15), by using a Taylor expansion for the logarithm, and by neglecting the q^4 terms, we conclude

$$\log(R(\Delta)) = -q^2\Delta D^{(2)}_{\text{ADC}}(\Delta), \tag{3.2.16}$$

where $R(\Delta)$ is the normalized signal.

3.3 Higher Order Moment: Kurtosis

In Section 1.2.1, we introduced some basic concepts of probability theory. In this section, we extend the description of the kurtosis and apply that to the measurement of the displacement of water particles in the tissues. Mathematically, the kurtosis, is expressed as [33]

$$K = \frac{\mu_4}{\mu_2^2} - 3 = \frac{k_4}{k_2^2}, \tag{3.3.1}$$

where μ_n and k_n are the n^{th} order moments and cumulants of the PDF, respectively. Subtracting three from the ratio of the fourth moment and the second moment squared in (3.3.1) results in the kurtosis of a Gaussian distribution being zero. As with the third moment (see Section 1.2.1), the kurtosis is a descriptor of the shape of the probability density function. The most common interpretation of kurtosis of a PDF is as a measure of the width of the peak, the contributions of the tails and any "shoulders"(i.e., subsidiary peaks). Having introduced the definition and explained the meaning of the kurtosis, now we will show how to use it to obtain a higher moment expression for the Apparent Diffusion Coefficient that, we hope, will give a deeper insight into the tissue structures.

3.3.1 Computing the ADC using higher order terms

To see how we can infer more information about the structure of the system by including the notion of kurtosis in a DWI experiment, we need an expression to relate the relative echo height to the higher order moments. As we saw at the beginning of this chapter, the relative echo height for a source of molecules that starts at the point ζ_0 is given by (3.1.1). By expanding the $\cos[q(x-\zeta_0)]$ in this equation as a Taylor

series up to the fourth order we get

$$\begin{aligned}
R(\Delta) &= \frac{1}{L(\Omega)} \int_{\Omega^-}^{\Omega^+} \int_{\Omega^-}^{\Omega^+} \rho(\zeta_0|x,\Delta) \cos[q(x-\zeta_0)] dx d\zeta_0, \\
&\sim \frac{1}{L(\Omega)} \int_{\Omega^-}^{\Omega^+} \int_{\Omega^-}^{\Omega^+} \rho(\zeta_0|x,\Delta) \left[1 - q^2 \frac{(x-\zeta_0)^2}{2!} + q^4 \frac{(x-\zeta_0)^4}{4!} + \cdots \right] dx d\zeta_0, \\
&\sim \frac{1}{L(\Omega)} \int_{\Omega^-}^{\Omega^+} \int_{\Omega^-}^{\Omega^+} \rho(\zeta_0|x,\Delta) dx d\zeta_0 - \frac{1}{L(\Omega)} \int_{\Omega^-}^{\Omega^+} \int_{\Omega^-}^{\Omega^+} \rho(\zeta_0|x,\Delta) q^2 \frac{(x-\zeta_0)^2}{2!} dx d\zeta_0 + \\
&\quad + \frac{1}{L(\Omega)} \int_{\Omega^-}^{\Omega^+} \int_{\Omega^-}^{\Omega^+} \rho(\zeta_0|x,\Delta) q^4 \frac{(x-\zeta_0)^4}{4!} dx d\zeta_0 + \mathcal{O}(x-\zeta_0)^6, \\
&\sim 1 - \frac{1}{L(\Omega)} \int_{\Omega^-}^{\Omega^+} \int_{\Omega^-}^{\Omega^+} \rho(\zeta_0|x,\Delta) q^2 \frac{(x-\zeta_0)^2}{2!} dx d\zeta_0 + \\
&\quad + \frac{1}{L(\Omega)} \int_{\Omega^-}^{\Omega^+} \int_{\Omega^-}^{\Omega^+} \rho(\zeta_0|x,\Delta) q^4 \frac{(x-\zeta_0)^4}{4!} dx d\zeta_0 + \mathcal{O}(x-\zeta_0)^6.
\end{aligned} \tag{3.3.2}$$

In (3.3.2), the term $\mathcal{O}(x-\zeta_0)^6$ involves an integral, and, therefore, depends on the value of the Displacement Probability Density Function $\rho(\zeta_0|x,\Delta)$ near $(x-\zeta_0)$. In fact, even though the PDF reaches some high values in the neighbourhood of the starting point ζ_0, due to the presence of obstacles and semi-permeable barriers in the great majority of the the domain, the value of $\rho(\zeta_0|x,\Delta)$ at the distance $(x-\zeta_0)$ is small. Thus we may expect the term that gathers the higher order terms in the Taylor expansion to be small. However, we will see below that, depending on the value of q that may not be the case (see Section 5.4).

It is useful to point out that, because the size of the imaged volume element is much bigger than the scale of the tissue microstructures, we can neglect any asymmetry in the displacement PDF and expand the previous series ignoring the odd terms [33]. Using the result in (1.2.6) we can rewrite (3.3.2) as a summation of moments. Taking the logarithm (3.2.13) we can write

$$\begin{aligned}
\log(R(\Delta)) &= -\frac{1}{L(\Omega)} \int_{\Omega^-}^{\Omega^+} \int_{\Omega^-}^{\Omega^+} \rho(\zeta_0|x,\Delta) q^2 \frac{(x-\zeta_0)^2}{2!} dx d\zeta_0 + \\
&\quad + \frac{1}{L(\Omega)} \int_{\Omega^-}^{\Omega^+} \int_{\Omega^-}^{\Omega^+} \rho(\zeta_0|x,\Delta) q^4 \frac{(x-\zeta_0)^4}{4!} dx d\zeta_0 + \mathcal{O}(q^2+q^4)^2, \\
&= \frac{-\mu_2 q^2}{2!} + \frac{\mu_4 q^4}{4!} + \mathcal{O}(q^2+q^4)^2
\end{aligned} \tag{3.3.3}$$

In theory, under the assumption that the PDF $\rho(\zeta_0|x,\Delta)$ is known a priori, (3.3.3) can be used to compute $R(\Delta)$. Because we are considering an extra term in the Taylor expansion, it is logical to assume that this measure for the signal would be more accurate. Once we have computed an expression for the signal from (3.3.3), we can compute a new, updated, value for the ADC using (3.2.16). To avoid confusion, we will use the notation $D^{(4)}_{\text{ADC}}$ to define the Apparent Diffusion Coefficient calculated from the signal using a fourth order Taylor expansion.

Chapter 4
Simplified models of cellular media

In Section 2.2 we discussed the inhomogeneity of human tissue due to compartmentalization that characterizes cellular and extracellular anatomy. However, the theory around Diffusion Weighted Imaging uses the strong assumption of homogeneity to compute the Apparent Diffusion Coefficient directly from the measured MRI signal.

We begin this chapter by developing two models for an idealized tissue in which we will study diffusion of water molecules in an inhomogeneous medium. Next we introduce the governing equations that describe diffusion in these models and suggest efficient numerical methods for their solution. For both models, the spatial discretization of the partial differential equations (PDEs) is done using a second-order finite-difference scheme. We solve the resulting equations by applying the Crank-Nicholson numerical scheme. This produces a linear system of equations from which we can compute the evolution in time of the DPDF for each point in the mesh grid. In the last part of this chapter we propose a different way of computing the ADC than the one presented in Chapter 3 which is hoped to capture the effect of the inhomogeneities in the models. We present the results of the simulations for different computational and physiological parameters in Chapter 5.

4.1 Idealized Tissue Model

The model we develop describes the restricted diffusion of particles, e.g., water molecules, in a cellular medium. In order to do this, a coupled one-dimensional model is created that is hoped to capture the general behaviour of a collection of cells contained within semi-permeable membranes and separated by extracellular space. One of the reasons

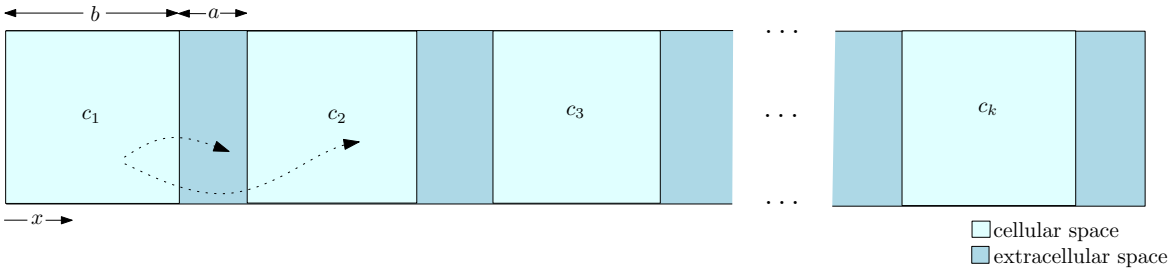

Figure 4.1: Cartoon of a system of cells. The extracellular and intracellular space are separated by semi-permeable barriers. The dashed lines represents some of the possible paths a particle can experience while diffusing.

why we consider a 1D model, is that DWI only measures displacement in a single direction at a time; therefore, a single-dimensional system seems justifiable. Initially, we consider diffusion across $2k$ regions alternating one-dimensional intervals of intracellular and extracellular space (as shown in Figure 4.1). The lengths of these two regions are generally different, and denoted by a and b for extra- and intracellular space, respectively. Because, as seen in Section 2.1, the inner structure of a cell is different from the extracellular space, we consider that the interior and exterior spaces also have different diffusion coefficients: D_1 for outside the cell, and D_2 for inside the cell. Cell membranes are modelled as semi-permeable walls with permeability coefficient p.

After, we extend this model by coupling the one-dimensional cell lattice with a one-dimensional channel of exclusively extracellular space (see Figure 4.3). In this way, we may also capture the transfer of molecules between non-adjacent cells.

A note about the terminology

To avoid confusion throughout the following chapters, it is appropriate to clarify some details about the terminology used to describe the model. We use the term *cellular channel* or *channel with cells* to indicate that portion of domain that includes alternating regions of cellular and extracellular space (see Figure 4.1). In a similar way, we define the part of the extended domain without cells *extracellular channel* or *channel of exclusively extracellular space* (see Figure 4.3). The word *region* is used uniquely for the cellular channel and denotes the portion of domain within two interfaces (cellular

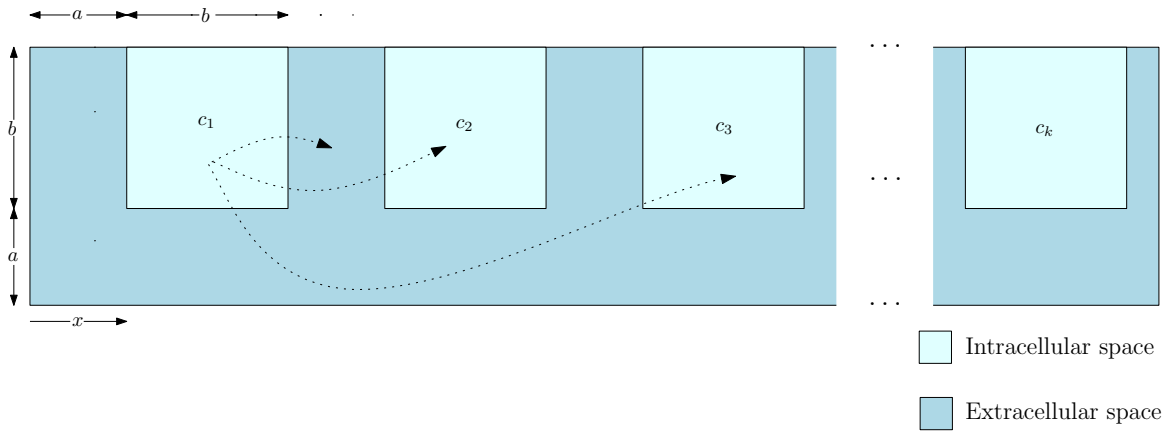

Figure 4.2: Cartoon of a system of cells with a channel of extracellular space. The cells are separated from the extracellular space via semi-permeable barriers. The dashed lines represent potential trajectories of diffusing particles.

barriers). Because, in the cellular channel, all cellular and extracellular regions alternate arranged on a periodic lattice, we use the word *lattice unit* to describe a portion of domain that includes a single cellular region *and* a single extracellular region.

4.1.1 Model assumptions

To simplify our model, we assume homogeneity both inside and outside cells, while the overall inhomogeneity of the tissue is modelled by the separation of the extracellular and intracellular space with semi-permeable interfaces which model cell walls. This model is not entirely realistic for two main reasons: first, as explained in Section 2.1, the presence of larger molecules and structures within cells makes the medium not homogenous. However, we assume that these smaller scale inhomogeneities are less important, and less structured, than the inhomogeneity introduced by the cell membranes. Secondly, it is well known that the cells in tissues are not arranged on a periodic lattice as in our model.

The justification for this model is that we can still represent the overall effect of the cellular membranes as well as restricted diffusion inside the cell by selecting appropriate permeability coefficients for the membrane and characteristic diffusion coefficients to model the displacement of a water molecule outside the cell.

4.2 Governing Equations for a System of Cells

As discussed in Section 2.2, the displacement probability of a proton diffusing in the i^{th} region is described by the 1D diffusion equation

$$\frac{\partial \rho_i}{\partial t} = D_i \frac{\partial^2 \rho_i}{\partial x^2}, \tag{4.2.1}$$

where the suffix $i = 1 \dots k$ is used to distinguish the different units of the cell lattice, and D_i is equal to D_1 if i is odd and to D_2 if i is even. Each region has its own coordinates with $x \in (0, L_i)$, where L_i is b if i is odd, and a if i is even. At the external boundaries of the system we prescribe the flux, so we can define pure constant Neumann boundary conditions:

$$\begin{aligned} \left.\frac{\partial \rho_1}{\partial x}\right|_{x=0} &= g_0, \\ \left.\frac{\partial \rho_{2k}}{\partial x}\right|_{x=\chi} &= g_\chi, \end{aligned} \tag{4.2.2}$$

where 0 and χ are the endpoints of the domain (i.e., $0 \leq x \leq \chi$). Below we will assume no flux through the external boundaries, i.e., we set $g_0 = g_\chi = 0$. In Section 4.1 it is stated that the two different types of regions in the domain are separated by a semi-permeable membrane situated at $x = L_i$. To study diffusion across the entire domain, we need to couple the two regions using two conditions at the interface. These interface conditions describe the likelihood of particles passing through semi-permeable membranes (Section 2.1). The coupling equations at the interfaces are

$$\begin{aligned} D_i \left.\frac{d\rho_i}{dx}\right|_{x=L_i} &= D_{i+1} \left.\frac{d\rho_{i+1}}{dx}\right|_{x=0}, \\ D_i \left.\frac{d\rho_i}{dx}\right|_{x=L_i} &= p\left(\rho_{i+1}(0,t) - \rho_i(L_i,t)\right), \end{aligned} \tag{4.2.3}$$

where p is the permeability of the membrane. The first equation describes the conservation of mass across the interfaces, that is, the flux of particles traversing from left to right is equal to the flux from right to left. The second condition expresses that the molecular flux across the interfaces is proportional to the magnitude of the jump discontinuity in density across the interface (the constant of proportionality being the permeability p associated with the membrane).

4.3 Discretizing the Governing Equations for the System of Cells

With the governing PDE established, we can construct an appropriate spatial and temporal discretization.

We choose to use a second-order centred finite-difference scheme for the spatial discretization. This takes us from a system of PDEs to a system of ODEs, where the time is the only independent variable. Then, the time-stepping is done by using the Crank-Nicolson method.

4.3.1 Space discretization

To solve this problem numerically, we discretize in space first: we discretize the different regions into a set of equally spaced points: that is, we discretize the intracellular region into n mesh points equally spaced by Δn (i.e. $\Delta n = b/n$) and we divide the extracellular space into m points separated by Δm (i.e. $\Delta m = a/m$). To keep the notation from becoming cumbersome, from now on we will identify the n points in the i^{th} intracellular region with the vector Φ_i:

$$\Phi_i = \begin{pmatrix} u(0) \\ u(\Delta n) \\ u(2\Delta n) \\ \vdots \\ u((n-1)\Delta n) \\ u(n\Delta n) \end{pmatrix} \qquad i = 0, 2, 4, .., k, \tag{4.3.1}$$

where $u(j\Delta n)$ for $j = 0, .., n$ represents approximations of the solution at the corresponding mesh points.

Similarly, the m points in the i^{th} extracellular space can be identified with the

vector Θ_i:

$$\Theta_i = \begin{pmatrix} v(0) \\ v(\Delta m) \\ v(2\Delta m) \\ \vdots \\ v((m-1)\Delta m) \\ v(m\Delta m) \end{pmatrix} \qquad i = 1, 3, 5, .., k-1, \tag{4.3.2}$$

where $v(j\Delta m)$ for $j = 0, .., m$, represents of the solution at the corresponding grid points.

Using a second-order finite-difference approximation for a second-order spatial derivative, the discretized equations for all the interior points in the intracellular and extracellular regions are

$$\frac{du_j}{dt} = D_1 \frac{u_{j-1} - 2u_j + u_{j+1}}{(\Delta n)^2}, \quad \text{for} \quad 1 \le j \le n-1, \tag{4.3.3}$$

$$\frac{dv_j}{dt} = D_2 \frac{v_{j-1} - 2v_j + v_{j+1}}{(\Delta m)^2}, \quad \text{for} \quad 0 \le j \le m-1, \tag{4.3.4}$$

respectively, and where the index j refers to the mesh grid point. We need to be careful with the equation for the first and the last point on the domain:

$$\frac{du_0}{dt} = D_1 \frac{u_{-1} - 2u_0 + u_1}{(\Delta n)^2}, \tag{4.3.5}$$

$$\frac{dv_m}{dt} = D_2 \frac{v_{m-1} - 2v_m + v_{m+1}}{(\Delta m)^2}. \tag{4.3.6}$$

Specifically, u_{-1} and v_{m+1}, which are called ghost points, are external to the domain and must be eliminated. In particular, we use the pure Neumann boundary conditions to eliminate u_{-1} and v_{m+1} by discretizing the boundary conditions (4.2.3) to obtain

$$\begin{aligned} \frac{u_1 - u_{-1}}{2\Delta n} &= g_0, \\ \frac{v_{m+1} - v_{m-1}}{2\Delta m} &= g_\chi. \end{aligned} \tag{4.3.7}$$

Solving (4.3.7) for u_{-1} and v_{m+1}, we get

$$\begin{aligned} u_{-1} &= -2\Delta n g_0 + u_1, \\ v_{m+1} &= 2\Delta m g_\chi + v_{m-1}. \end{aligned} \tag{4.3.8}$$

Using these results, we can rewrite (4.5.2) and (4.5.3) for the point u_0 and v_m as:

$$\begin{aligned}\frac{du_0}{dt} &= D_1\frac{2u_0 - 2u_1}{(\Delta n)^2} - \frac{2g_0}{\Delta n},\\ \frac{dv_m}{dt} &= D_2\frac{-2v_{m-1} + 2v_m}{(\Delta m)^2} + \frac{2g_\chi}{\Delta m}.\end{aligned} \tag{4.3.9}$$

Similarly, discretization in each compartment of the domain leads to the presence of ghost points corresponding to the interfaces of adjacent regions. We can eliminate the ghost points across the domain, by discretizing the boundary conditions (4.2.3) for the internal membranes. The boundary condition at each coordinate $x = L_i$ can be written as:

$$\begin{aligned}D_1\frac{u_{n+1} - u_{n-1}}{2\Delta n} - D_2\frac{v_1 - v_{-1}}{2\Delta m} &= 0,\\ D_1\frac{u_{n+1} - u_{n-1}}{2\Delta n} - p(v_0 - u_n) &= 0, \qquad \text{if } i \text{ is odd,}\end{aligned} \tag{4.3.10}$$

and as

$$\begin{aligned}D_2\frac{v_{n+1} - v_{n-1}}{2\Delta m} - D_1\frac{u_1 - u_{-1}}{2\Delta n} &= 0,\\ D_2\frac{v_{n+1} - v_{n-1}}{2\Delta m} - p(u_0 - v_n) &= 0, \qquad \text{if } i \text{ is even.}\end{aligned} \tag{4.3.11}$$

Assuming here that we consider just the case where a cell region is on the left side of a extracellular region, solving (4.3.10) for u_{n+1} allows us to rewrite the discretized equations for the point u_n on the the left edge of the membrane as

$$\begin{aligned}\frac{du_n}{dt} &= D_1\frac{u_{n-1} - 2u_n + u_{n+1}}{(\Delta n)^2}\\ &= \frac{2D_1}{\Delta n^2}u_{n-1} - \left(\frac{2D_1}{\Delta n^2} + \frac{2p}{\Delta n}\right)u_n + \frac{2p}{\Delta m}v_0.\end{aligned} \tag{4.3.12}$$

In the same way we can get an expression for the right point on the membrane. Substituting the expression for v_{-1} in the discretized equation for the point v_0, we get:

$$\begin{aligned}\frac{dv_0}{dt} &= D_1\frac{u_{-1} - 2v_0 + v_1}{(\Delta m)^2}\\ &= \frac{2p}{\Delta n}u_n - \left(\frac{2D_2}{\Delta m^2} + \frac{2p}{\Delta m}\right)v_0 + \frac{2D_2}{\Delta m^2}v_1.\end{aligned} \tag{4.3.13}$$

Similar derivation could be done in the case where a cellular region is on the right of an extracellular region. It is more convenient to stack the vectors Φ_i and Θ_i to create

a single vector that contains all the unknowns. We then define a vector W

$$W = \begin{pmatrix} u_0(0) \\ u_0(\Delta n) \\ \vdots \\ u_0(n\Delta n) \\ v_1(0) \\ v_1(\Delta m) \\ \vdots \\ v_1(m\Delta m) \\ u_2(0) \\ \vdots \end{pmatrix}, \tag{4.3.14}$$

where the suffix refers to the number of the corresponding region of intracellular or extracellular space in our domain. The RHS from the Neumann boundary conditions are included in a column vector G; we choose the prescribed fluxes at the left- and right-hand point of the domain to be zero, therefore G is the zero vector. We can now rewrite the initial PDE for our problem as a set of ODEs which has the form

$$\frac{dW}{dt} = A\ W + G. \tag{4.3.15}$$

In (4.3.15), A is a the matrix of the finite difference discretization. If, just for now, we suppose that our domain consists of a single lattice unit (i.e. one cell with some extracellular space on its right side), then the matrix A is given by

$$A = \left(\begin{array}{cccc|cccc} (-2)\frac{D_1}{\Delta n^2} & (2)\frac{D_1}{\Delta n^2} & 0 & \dots & 0 & 0 & \dots & 0 \\ 1\frac{D_1}{\Delta n^2} & (-2)\frac{D_1}{\Delta n^2} & 1\frac{D_1}{\Delta n^2} & 0 & 0 & \dots & \dots & 0 \\ 0 & \dots & \dots & \dots & \dots & \dots & \dots & \dots \\ 0 & 0 & 2\frac{D_1}{\Delta n^2} & (-2)\frac{D_1}{\Delta n^2} - \frac{2p}{\Delta n} & \frac{2p}{\Delta m^2} & \dots & 0 & 0 \\ \hline 0 & 0 & 0 & \frac{2p}{\Delta n^2} & -2\frac{D_2}{\Delta m^2} - \frac{2p}{\Delta m} & (-1)\frac{D_2}{\Delta m^2} & 0 \dots & \\ 0 & 0 & 0 & 0 & 1\frac{D_2}{\Delta m^2} & (-2)\frac{D_2}{\Delta m^2} & 1\frac{D_2}{\Delta m^2} & 0 \\ \dots & \dots & \dots & \dots & \dots & \dots & \dots & \dots \\ 0 & 0 & \dots & 0 & 0 & 0 & 2\frac{D_2}{\Delta m^2} & (-2)\frac{D_2}{\Delta m^2} \end{array}\right) \tag{4.3.16}$$

4.3.2 Time-stepping

Having completed the discretization in space, we have reduced the initial PDE to a set of ODEs. In order to find the numerical solution to the corresponding IVP we will use the Crank-Nicholson method as a time-stepper.

Using the Crank-Nicolson scheme we can rewrite the semi-discrete problem as

$$\frac{\vec{W}^{\tau+1} - \vec{W}^{\tau}}{\Delta t} = \frac{1}{2}(A\ \vec{W}^{\tau+1} + A\ \vec{W}^{\tau}) + G, \tag{4.3.17}$$

where the superscript τ refers to the time index. We would like to solve for $\vec{W}^{\tau+1}$, therefore, we rearrange the terms to obtain

$$(I - \frac{\Delta t}{2}\ A)\ \vec{W}^{\tau+1} = (I + \frac{\Delta t}{2}\ A)\ \vec{W}^{\tau} + G. \tag{4.3.18}$$

At each time step (4.3.18) must be solved for $\vec{W}^{\tau+1}$, i.e.,

$$\vec{W}^{\tau+1} = \left(I - \frac{\Delta t}{2}\ A\right)^{-1} \left[\left(I + \frac{\Delta t}{2}\ A\right)\ \vec{W}^{\tau} + G\right]. \tag{4.3.19}$$

Simulations can be found in Chapter 5.

4.4 Governing Equations for the Coupled System

Thus far, our system has been modelled as a 1D channel with alternating intra- and extra-cellular space. In this section, we extend the model by coupling this 1D channel of cells with a 1D channel consisting exclusively of extracellular space. The evolution of the displacement probability of a particle in the cell and channel regions is modelled with the one-dimensional diffusion equation. The diffusion equations are coupled through a term that is proportional to the difference of the density of particles in the cell and in the adjacent portion of extracellular channel region. To distinguish the different behaviour of particles in different domains, we decompose the total density ρ into β for the channel containing cells and γ for the extracellular channel. The equations become

$$\frac{\partial \beta}{\partial t} = D(x)\frac{\partial^2 \beta}{\partial x^2} + \alpha_1[\gamma - \beta] \tag{4.4.1}$$

and

$$\frac{\partial \gamma}{\partial t} = D_2\frac{\partial^2 \gamma}{\partial x^2} + \alpha_2[\beta - \gamma]. \tag{4.4.2}$$

Previously, the diffusion coefficient in the equation describing the behaviour of the molecules in the channel with cells depends on the spatial variable x, because in this channel we have alternating regions with different physical properties. Therefore, the diffusion coefficient $D(x)$ is either D_1 or D_2 depending on whether the coordinate x is inside or outside the cell. On the other hand, the diffusion coefficient in (4.4.2) is constant as we consider the channel of extracellular space as homogeneous. For the channel containing cells, the boundary conditions at the endpoints of the domain are the same as in Section 4.2, while for the extracellular channel we now have

$$\begin{aligned} D_2 \frac{\partial \gamma}{\partial x}\bigg|_{x=0} &= g_0, \\ D_2 \frac{\partial \gamma}{\partial x}\bigg|_{x=\chi} &= g_\chi, \end{aligned} \tag{4.4.3}$$

where 0 and χ are the external boundaries of the domain (i.e., $0 \leq x \leq \chi$).

4.4.1 Coupling the cellular and extracellular channels

Before discretizing the equations describing the cellular channel and the channel of just extracellular space, we complete our description of the model by deriving an expression for the coupling terms in (4.4.1) and (4.4.2) , namely $\alpha_1(x)$ and $\alpha_2(x)$. To do this, the two channels are each assigned their own vertical coordinates, taking $y = 0$ to correspond to the lower-most part of each of the two different channels. To eliminate the y dependence, we define a mean density that depends exclusively on the horizontal coordinate x and on the time t: $\bar{\beta}(x,t)$ and $\bar{\gamma}(x,t)$. In particular, for the cellular channel, assuming symmetry about $y = b/2$, the change for the mean density is

$$\begin{aligned} \frac{\partial \bar{\beta}}{\partial t} &= \frac{2}{b}\int_0^{\frac{b}{2}} \frac{\partial \beta}{\partial t}\partial y = \frac{2}{b}\int_0^{\frac{b}{2}} D(x)\left[\frac{\partial^2 \beta}{\partial x^2} + \frac{\partial^2 \beta}{\partial y^2}\right] dy, \\ &= D(x)\frac{\partial^2 \bar{\beta}}{\partial x^2} - \frac{2}{b}D(x)\frac{\partial \beta}{\partial y}\bigg|_{y=0}. \end{aligned} \tag{4.4.4}$$

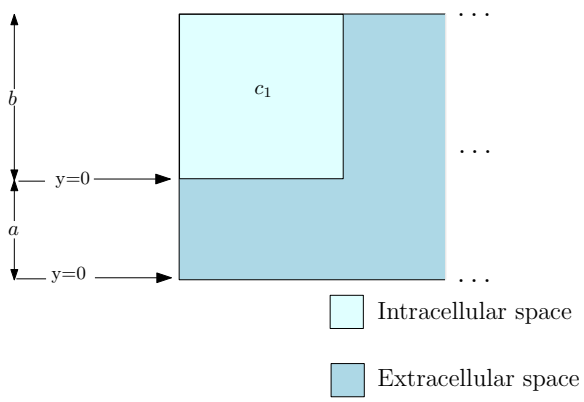

Figure 4.3: In the coupled system, we give to the cellular and extracellular channel each their own coordinates in the vertical direction. This is useful to eliminate y-dependence for the density of molecules moving from the channel with cells to the region of just extracellular space.

Similarly, for the extracellular channel, assuming symmetry about $y = a/2$, the change for the mean density is

$$\begin{aligned}\frac{\partial \bar{\gamma}}{\partial t} &= \frac{2}{a}\int_0^{\frac{a}{2}} \frac{\partial \gamma}{\partial t}\partial y = \frac{2}{a}\int_0^{\frac{a}{2}} D_2\left[\frac{\partial^2 \gamma}{\partial x^2} + \frac{\partial^2 \gamma}{\partial y^2}\right] dy, \\ &= D_2\frac{\partial^2 \bar{\gamma}}{\partial x^2} - \frac{2}{a}D_2\frac{\partial \gamma}{\partial y}\bigg|_{y=a}. \end{aligned} \tag{4.4.5}$$

Because we want to find an expression for the flux of particles between two channels, when x is such that there is no semi-permeable membrane between the two channels, we define the flux of molecules coming from the channel with cells at the interface to be $\frac{\partial \beta}{\partial y}\big|_{y=0} = 2(\bar{\beta} - \bar{\gamma})/(a+b)$. Substituting this into (4.4.4) we get

$$\frac{\partial \bar{\beta}}{\partial t} = D(x)\frac{\partial^2 \bar{\beta}}{\partial x^2} + \frac{4}{b(a+b)}D_2(\bar{\gamma} - \bar{\beta}). \tag{4.4.6}$$

Therefore $\alpha_1(x) = \frac{4}{b(a+b)}D_2$. Similarly we can derive an expression for $\alpha_2(x)$. We define the flux from the extracellular channel to the channel with cells to be $\frac{\partial \gamma}{\partial y}\big|_{y=a} = 2(\bar{\gamma} - \bar{\beta})/(a+b)$. Substituting this into (4.4.5) we get

$$\frac{\partial \bar{\gamma}}{\partial t} = D_2\frac{\partial^2 \bar{\gamma}}{\partial x^2} + \frac{4}{a(a+b)}D_2(\bar{\beta} - \bar{\gamma}). \tag{4.4.7}$$

Hence, $\alpha_2 = \frac{4}{a(a+b)}D_2$.

However, when the coordinate x is such that there is a membrane separating the channel with cells and the extracellular channel we use the following boundary condi-

tion:

$$D_1 \frac{\partial \beta}{\partial y}\bigg|_{y=0} = D_2 \frac{\partial \gamma}{\partial y}\bigg|_{y=a} = p(\beta^* - \gamma^*), \tag{4.4.8}$$

where β^* and γ^* are hypothetical densities at the interface. We define the flux of molecules coming from the channel with cells at the interface to be

$$\frac{\partial \beta}{\partial y}\bigg|_{y=0} = 2(\bar{\beta} - \beta^*)/b. \tag{4.4.9}$$

Following the same idea, the flux of particles from the extracellular channel to the channel with cells can be written as

$$\frac{\partial \gamma}{\partial y}\bigg|_{y=a} = 2(\gamma^* - \bar{\gamma})/a. \tag{4.4.10}$$

Solving (4.4.8)-(4.4.10) for $P(\beta^* - \gamma^*)$ yields

$$P(\beta^* - \gamma^*) = \frac{2pD_1D_2}{2D_1D_2 + p(aD_1 + bD_2)}(\bar{\beta} - \bar{\gamma}) \tag{4.4.11}$$

Using (4.4.11), we can rewrite (4.4.9) and (4.4.10) as:

$$\frac{\partial \beta}{\partial y}\bigg|_{y=0} = \frac{4pD_1D_2}{2D_1D_2 + p(aD_1 + bD_2)}\frac{(\bar{\gamma} - \bar{\beta})}{b}, \qquad \text{and,} \tag{4.4.12}$$

$$\frac{\partial \gamma}{\partial y}\bigg|_{y=a} = \frac{4pD_1D_2}{2D_1D_2 + p(aD_1 + bD_2)}\frac{(\bar{\beta} - \bar{\gamma})}{a}, \tag{4.4.13}$$

respectively. Substituting (4.4.12) into (4.4.4) we get:

$$\frac{\partial \bar{\beta}}{\partial t} = D(x)\frac{\partial^2 \bar{\beta}}{\partial x^2} + \frac{8pD_1D_2}{2bD_1D_2 + pb(aD_1 + bD_2)}D_1(\bar{\gamma} - \bar{\beta}). \tag{4.4.14}$$

Therefore we can conclude $\alpha_1(x) = \frac{8pD_1D_2}{2bD_1D_2+pb(aD_1+bD_2)}D_1$. In a similar way, substituting (4.4.13) into (4.4.5) we get

$$\frac{\partial \bar{\gamma}}{\partial t} = D_2\frac{\partial^2 \bar{\gamma}}{\partial x^2} + \frac{8pD_1D_2}{2aD_1D_2 + pa(aD_1 + bD_2)}D_2(\bar{\beta} - \bar{\gamma}). \tag{4.4.15}$$

Hence, in this case, $\alpha_2 = \frac{8pD_1D_2}{2aD_1D_2+pa(aD_1+bD_2)}D_2$.

4.5 Discretization of the Governing Equations for the Coupled System

Before discretizing using a finite-difference method, it is important to note that we choose the grid spacing in the extracellular channel to be the same as that of the cellular channel. This will facilitate the coupling of the two channels. This means

that the grid points in the extracellular channel are not all equally spaced, but when x corresponds to an intracellular region of the channel with cells the spacing between two points is going to be Δn, and when x corresponds to an extracellular region, the spacing is Δm.

We start by discretizing the diffusion equation for the cellular channel and the extracellular channel without the linear coupling terms. Next, we include these terms and thus couple the two channels.

4.5.1 Spatial discretization of the channel

We start by discretizing the governing equations for the cellular and extracellular channels as if they were uncoupled. In particular, the discretization for the channels with cells is the same as in Section 4.3 because we have the same lattice structure of cells and extracellular space separated by membranes modelled by (4.2.3). In the extracellular channel the equation for the uncoupled case is

$$\frac{\partial \gamma}{\partial t} = D_2 \frac{\partial^2 \gamma}{\partial x^2}. \tag{4.5.1}$$

If we discretize the entire domain into a set of η points, the equation for all the internal points in the channel, i.e., for $j = 1 : (\eta - 1)$, can be approximated using a second-order finite-difference scheme

$$\frac{d\gamma_j}{dt} = D_2 \frac{\gamma_{j-1} - 2\gamma_j + \gamma_{j+1}}{(\Delta n)^2}, \qquad \text{if } x \text{ corresponds to an intracellular region, and}$$

$$\frac{d\gamma_j}{dt} = D_2 \frac{\gamma_{j-1} - 2\gamma_j + \gamma_{j+1}}{(\Delta m)^2}, \qquad \text{if } x \text{ corresponds to an extracellular region.}$$

As in the channel with cells, because we are using Neumann boundary conditions, we need to be careful with the points γ_0 and γ_η. If the first region in the channel with cells corresponds to a cell, and the last one corresponds to extracellular space, then the equation for these points are respectively

$$\frac{d\gamma_0}{dt} = D_2 \frac{\gamma_{-1} - 2\gamma_0 + \gamma_1}{(\Delta n)^2}, \tag{4.5.2}$$

$$\frac{d\gamma_\eta}{dt} = D_2 \frac{\gamma_{\eta-1} - 2\gamma_\eta + \gamma_{\eta+1}}{(\Delta m)^2}. \tag{4.5.3}$$

To eliminate the two ghost points γ_{-1} and $\gamma_{\eta+1}$, we can discretize the boundary conditions (4.4.3)

$$\begin{aligned} \frac{\gamma_1 - \gamma_{-1}}{2\Delta n} &= g_0, \\ \frac{\gamma_{\eta+1} - \gamma_{\eta-1}}{2\Delta m} &= g_\chi, \end{aligned} \tag{4.5.4}$$

and solve (4.5.4) for γ_{-1} and $\gamma_{\eta+1}$. Using these results we can rewrite (4.5.2) and (4.5.3) as

$$\begin{aligned} \frac{d\gamma_0}{dt} &= D_2 \frac{2\gamma_0 - 2\gamma_1}{(\Delta n)^2} - \frac{2g_0}{\Delta n}, \qquad \text{and} \\ \frac{d\gamma_\eta}{dt} &= D_2 \frac{-2\gamma_{\eta-1} + 2v_\eta}{(\Delta m)^2} + \frac{2g_\chi}{\Delta m}. \end{aligned} \tag{4.5.5}$$

As stated above (see Section 4.1), we treat the extracellular channel as an homogeneous medium. Therefore, contrary to the channel with cells, we do not have permeable barriers throughout the domain. However, care must be taken at the points in the extracellular channel that corresponds to the barrier because, if $\Delta n \neq \Delta m$, the grid spacing changes at those points. Thus, upon discretization of (4.5.1) we obtain

$$\frac{d\Gamma}{dt} = C\ \Gamma + G, \tag{4.5.6}$$

where Γ is the vector of unknowns corresponding to the grid points. If we assume that there are just two different compartments in the channel with cells, then the vector of

unknowns for the extracellular channel would look like

$$\Gamma = \begin{pmatrix} \gamma(0) \\ \gamma(\Delta n) \\ \gamma(2\Delta n) \\ \vdots \\ \gamma((n-1)\Delta n) \\ \gamma(n\Delta n) \\ \gamma(\Delta m) \\ \gamma(2\Delta m) \\ \vdots \\ \gamma((m-1)\Delta m) \\ \gamma(m\Delta m) \end{pmatrix}. \tag{4.5.7}$$

In equation (4.5.6), G is, again, a vector that accounts for the boundary conditions. Since we choose the prescribed flux at the boundaries to be zero, (i.e., $g_0 = 0$ and $g_\chi = 0$), G is the zero vector.

4.6 Discretization of the Governing Equation for the Whole System

In order to see better how the discretization for the whole system works, it is useful to rewrite the previous equations as

$$\frac{\partial \beta}{\partial t} = D(x)\frac{\partial^2 \beta}{\partial x^2} - \alpha_1 \beta + \alpha_1 \gamma, \tag{4.6.1}$$

$$\frac{\partial \gamma}{\partial t} = D_2\frac{\partial^2 \gamma}{\partial x^2} - \alpha_2 \gamma + \alpha_2 \beta. \tag{4.6.2}$$

First consider (4.6.1), which models the behaviour of the molecules in the cellular channel. The first two terms, which involve derivatives with respect to β, model the diffusion in the channel with cells as if there is no extracellular channel. In order to take into account the coupling with the extracellular channel, we need to discretize the third and the fourth term in the same equation. Those term can be represented via a diagonal matrix with alternating coefficients $\frac{8pD_1D_2}{2bD_1D_2+pb(aD_1+bD_2)}D_1$ and $\frac{4}{b(a+b)}D_2$

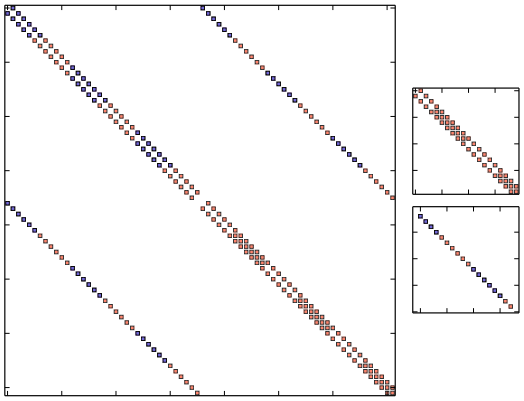

Figure 4.4: Structure of the entire matrix Λ after the discretization. The frames the right display zooms on the main diagonal (top) and of the off diagonal bands (bottom). From now on, unless specified, the blue and orange diamonds correspond to intracellular and extracellular space respectively.

on the main diagonal depending on whether there is a semi-membrane at the interface between the two channels. We proceed in a similar manner in the discretization of (4.6.2). The first two terms in (4.6.2) model the diffusion process in the channel. The third and fourth terms describe the coupling with the cellular channel and, when discretized as diagonal matrices with the factors $\frac{8pD_1D_2}{2aD_1D_2+pa(aD_1+bD_2)}D_2$ and $\frac{4}{a(a+b)}D_2$ on the main diagonal depending on the presence of a membrane between the two channels.

With all terms in the governing equations discretized, the discretized system has the form:

$$\frac{d\Sigma}{dt} = \Lambda\Sigma + G. \tag{4.6.3}$$

The structure of the entire matrix of the discretization Λ is shown in Figure 4.4.The entries in the band along the main diagonal represent the discretized uncoupled terms as they are in the uncoupled equations, while the coupling terms are found in the off-diagonal bands .

(a) (b)

Figure 4.5: Order of the unknows in the system before (a) and after (b) applying the permutation matrix

4.6.1 Change of the structure of the matrix

Solving a system with a matrix like the one in Figure 4.4 might be quite expensive and inefficient; in fact it is easy to see that the matrix has a sparse structure, but the entries are not all clustered around the main diagonal. To increase the efficiency and speed of computation we can significantly reduce the band-width by interchanging the order of the columns and the rows in the whole system. The unknowns and the equations in the system can be rearranged by using a permutation matrix P. This matrix is built so that the unknowns for the cellular and extracellular channels corresponding to the same grid point become adjacent. Figure 4.5 displays the order of the unknowns in the system of equations before (Figure 4.5a) and after (Figure 4.5b) applying the permutation matrix.

We start by rearranging the columns of Λ which corresponds to rearranging the order of the unknowns in the system. This is equivalent to multiplying the matrix Λ on the right by a particular permutation matrix P. After doing this, using the Crank-Nicolson method to time-step our solution as we did in section 4.3.2, the system we have to solve is

$$(I - \frac{\Delta t}{2}\ \Lambda P_c)\ \vec{W}^{\tau+1} = (I + \frac{\Delta t}{2}\ \Lambda P_c)\ \vec{W}^{\tau} + \vec{G}, \tag{4.6.4}$$

where P_c is the permutation matrix that acts on the columns of Λ and the suffix τ denotes the time-step. The structure of the matrix, after this operation, is represented in Figure 4.6.

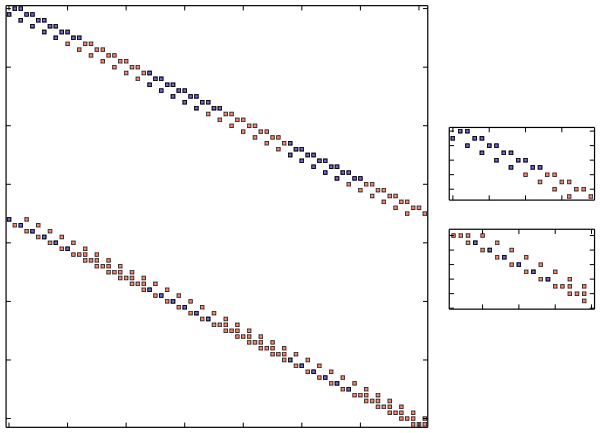

Figure 4.6: Structure of the entire matrix after swapping the columns. The frames on the right display zooms of the matrix structure.

In order to obtain a matrix that is banded, we apply another permutation to the rows to our system. This is equivalent to multiplying the system on the left by a permutation matrix P_r. In our case, to obtain a banded matrix, P_r is equivalent to P_c^T. Applying this permutation corresponds to the following operation on the system (4.6.4) we obtain

$$(I - \frac{\Delta t}{2}\ P_r \Lambda P_c) P_r\ \vec{W}^{\tau+1} = (I + \frac{\Delta t}{2}\ P_r \Lambda P_c)\ P_r \vec{W}^{\tau} + \vec{G}. \tag{4.6.5}$$

The structure of the matrix after applying the permutation is presented in Figure 4.7.

4.7 The Apparent Diffusion Coefficient

In Section 3.2, we define the ADC and the means by which to compute it from an MRI signal. Here, we derive an expression for the ADC starting from the Einstein relation for diffusion and we justify the use for our model.

4.7.1 The ADC from the Einstein relation for diffusion

The one-dimensional diffusion equation can be written as

$$\frac{\partial \rho(\zeta_0|x,t)}{\partial t} = D \frac{\partial^2 \rho(\zeta_0|x,t)}{\partial x^2}, \tag{4.7.1}$$

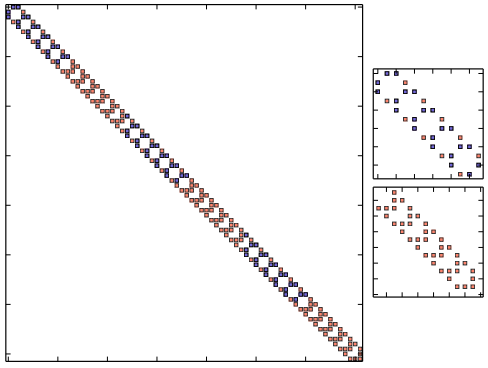

Figure 4.7: Structure of the entire matrix after swapping the columns and the rows. The matrix is now banded around the main diagonal. The structure of the different parts of the main diagonal is displayed in the frames on the right.

where $\rho(\zeta_0|x,t)$ is the conditional probability that a particle starting at ζ_0 will be at position x after a time t, and D is the diffusion coefficient. To show that (4.7.1) can describe diffusive behaviours, we consider the mean square displacement of a particle described by: $\left\langle (x(t)-\zeta_0(t))^2 \right\rangle \sim t$.

Molecular dynamics theory allows us to express the mean square displacement of a particle that starts diffusing at ζ_0 as [36] [22]

$$\left\langle (x-\zeta_0)^2 \right\rangle = \int_{-\infty}^{+\infty} dx (x-\zeta_0)^2 \rho(\zeta_0|x,t). \tag{4.7.2}$$

Multiplying (4.7.1) by $(x-\zeta_0)^2$ and integrating over the whole line we can rewrite (4.7.2) as

$$\underbrace{\frac{\partial}{\partial t}\int_{-\infty}^{+\infty} dx (x-\zeta_0)^2 \rho(\zeta_0|x,t)}_{\text{LHS}} = \underbrace{D\int_{-\infty}^{+\infty} dx (x-\zeta_0)^2 \frac{\partial^2 \rho(\zeta_0|x,t)}{\partial x^2}}_{\text{RHS}} \tag{4.7.3}$$

Using (4.7.2) we can rewrite the LHS in (4.7.3) as

$$\frac{\partial}{\partial t}\int_{-\infty}^{+\infty} dx (x-\zeta_0)^2 \rho(\zeta_0|x,t) = \frac{\partial}{\partial t}\left\langle (x-\zeta_0)^2 \right\rangle. \tag{4.7.4}$$

To simplify the integral on the RHS in (4.7.3), we use integration by parts to get [22]

$$D\int_{-\infty}^{+\infty} dx(x-\zeta_0)^2\frac{\partial^2\rho(\zeta_0|x,t)}{\partial x^2} = \underbrace{D(x-\zeta_0)^2\frac{\partial\rho(\zeta_0|x,t)}{\partial x}\Big|_{-\infty}^{+\infty}}_{1} - \underbrace{D\int_{-\infty}^{+\infty}\frac{\partial(x-\zeta_0)^2}{\partial x}\frac{\partial\rho(\zeta_0|x,t)}{\partial x}dx}_{2}. \tag{4.7.5}$$

Making use of the properties of a PDF in 1.2.1 and applying L'Hôpital's rule, the first term on the RHS of (4.7.5) is zero

$$D(x-\zeta_0)^2\frac{\partial\rho(\zeta_0|x,t)}{\partial x}\Big|_{-\infty}^{+\infty} = 0. \tag{4.7.6}$$

We can integrate by parts again to Integral 2 to get [22]

$$-2D\int_{-\infty}^{+\infty}(x-\zeta_0)\frac{\partial\rho(\zeta_0|x,t)}{\partial x}dx = \underbrace{-2D(x-\zeta_0)\rho(\zeta_0,x,t)\Big|_{-\infty}^{+\infty}}_{3} + \underbrace{2D\int_{-\infty}^{+\infty}\frac{\partial(x-\zeta_0)}{\partial x}\rho(\zeta_0|x,t)dx}_{4}. \tag{4.7.7}$$

Integral 3 goes to 0 for the same reasons as integral 1

$$-2D(x-\zeta_0)\rho(\zeta_0,x,t)\Big|_{-\infty}^{+\infty} = 0. \tag{4.7.8}$$

Integral 4 simply becomes

$$2D\int_{-\infty}^{+\infty}\rho(\zeta_0|x,t)dx = 2D. \tag{4.7.9}$$

When we put back the LHS and the RHS of (4.7.3) together we get

$$\frac{\partial}{\partial t}\left\langle(x-\zeta_0)^2\right\rangle = 2D. \tag{4.7.10}$$

(4.7.10) is a separable ODE. Rearranging the terms and integrating over the time we can write

$$\left\langle(x-\zeta_0)^2\right\rangle = 2Dt. \tag{4.7.11}$$

Using (4.7.2), we get an expression for the diffusion coefficient

$$D = \frac{1}{2t}\int_{-\infty}^{+\infty} dx(x-\zeta_0)^2\rho(\zeta_0|x,t). \tag{4.7.12}$$

In the case where the domain is homogenous this integral will produce a constant

equal to the diffusion coefficient D independent of ζ_0. However, in the case where the domain is not homogenous the value of this integral will depend on both time and ζ_0. It make sense, then, to average of ζ_0 and use this average quantity as definition of an ADC. Thus we may evaluate the integral in (4.7.12) over every region of the lattice to obtain:

$$D = \frac{1}{2t}\int_{-\infty}^{+\infty}\int_{-\infty}^{+\infty}(x-\zeta_0)^2\rho(\zeta_0|x,t)d\zeta_0 dx. \tag{4.7.13}$$

Because the lattice is periodic, the average over a single lattice unit gives the average over the whole domain. The inner integral in this case can be evaluated from 0 to α, is α is the lattice constant, and the integral then becomes

$$D_{\text{AVE}} = \frac{1}{2t\alpha}\int_0^{\chi}\int_0^{\alpha} dx d\zeta_0 (x-\zeta_0)^2\rho(\zeta_0|x,t) \tag{4.7.14}$$

where D_{AVE} represents now the apparent diffusion coefficient for our model.

Chapter 5

Results

In Chapter 4, we introduced the model used in this study to reproduce the diffusion of water molecules in an inhomogeneous medium. In this chapter, we present some numerical tests we performed to establish the proposed model's validity and applicability to simulating diffusion in cellular media.

In Section 5.1, we consider a simple problem in which the same is taken diffusion coefficient across the entire domain and the intracellular and extracellular regions have the same width. Although the specific parameters chosen for this test do not resemble the physiological reality of a system of cells, the results obtained are qualitatively accurate and validate the correctness of the model. In Section 5.2 we perform additional tests to verify the reliability and numerical accuracy of the code and we justify the choice of the size of the computational domain. In Section 5.3, we present the shape of the DPDF for a inhomogeneous media. While the computational parameters are chosen to be the same for each case, examples of different cellular configurations are presented by changing physiological parameters such as the width of the cellular and extracellular regions and the membranes permeability. The DPDFs for each case of the diffusion problem are presented as well. Given the numerical solutions to the PDE model, Section 5.4 covers the core of this project. Here we present various computations of the ADC using different approaches presented in Sections 3.2.2, 3.3.1 and 4.7. For each case, we justify the differences and validity in the various strategies for computing the ADC in the presence of inhomogeneities.

5.1 Preliminary Tests

We begin this chapter with a validation of the code for the discretization of the governing equations as explained in Section 4.2. First we make a qualitative and quantitative comparison of our results with those obtained by J. E. Tanner [31]. In his original work, Tanner showed the form of the Displacement Probability Density Function of particles randomly diffusing from a Dirac Delta function initial condition in a system of parallel planar, equally-spaced, semi-permeable barriers. Tanner, to model the diffusion in his inhomogeneous system, used a series of eigenfunctions for $\rho(x,t)$ to compute the shape of the DPDF [31]. Here, we use a different approach; see Chapter 4. We compute the shape of the DPDF for different values of the membrane permeability p and diffusion time t, and we will justify how the results we obtain represent a good qualitative comparison with the ones obtained in the original work.

The geometry of the domain is the same for all the cases presented in this section. Specifically, we consider a finite number, N, of one-dimensional equally-spaced regions separated by semi-permeable barriers. As explained in Section 4.1, the cells are assumed to be arranged on a periodic lattice with lattice constant α. In order to be able to do a more meaningful comparison, we choose to use the same values for the lattice constant, diffusion coefficients, permeability and diffusion times as Tanner [31]. Thus, for the comparison, each region, corresponding to both intracellular or extracellular space, has length $l = 1.5\mu$m. It follows that the lattice constant α for this problem is equal to 3μm. Similarly, we choose the diffusion coefficient $D = 0.5$ cm^2/s $\times 10^{-5}$ in both the intracellular and extracellular regions. We make the comparison at several diffusion times t and for two different values of the permeability of the barriers. A summary of the system parameters used in the comparison is presented in Table 5.1.

The original work of Tanner reported the number of intracellular and extracellular region used for the calculation and the form of the initial condition, but there was no indication of how many terms were used in the eigenfuction expansion to compute the shape of the DPDF. We choose again to use the same number of regions in our domain and we discretize each region into 40 grid points. The Initial Condition (IC)

System parameters	Value used by both Tanner [31] and us
Lattice constant α, μm	3
Diffusion coefficient D, cm^2/s $\times 10^{-5}$	0.5
Diffusion times t, msec	1.8-180
Permeability p, cm/s	0.009-0.03

Table 5.1: Range of biological parameters relative to a single cell used in comparison with Tanner [31]

Numerical Simulation Parameters	Value used by us
Number of regions, N	20
Number of grid point for each region, nx	40
Number of time steps, nT	1.8e7, 1.8e8, 1.8e9
Time step, Δt	1e-9
Mean of the IC, μ	1.42308e-8
Standard Deviation of the IC, σ	9e-6

Table 5.2: Range of parameters used in the numerical simulation to reproduce Tanner's original work [31].

is taken to be a very steep and narrow Gaussian distribution which should approximate a Dirac Delta function. The IC is defined using the built-in Python function scipy.stats.norm.pdf with mean corresponding to the grid point x_0 at the centre of the middle region of the domain and variance $\sigma = 2Dt$, where t is some very short diffusion time (see Section 2.2.2). A summary of the parameters used in the numerical simulation is reported in Table 5.2.

The solutions generated with the IC described above are presented in Figure **??** for different values of the reduced time $T \equiv Dt/\alpha^2$ and reduced permeability $P \equiv \alpha p/D$. The solutions have a single maximum and decrease monotonically on the left and on the right. Because we choose the source of particles diffusing to be in the centre of the domain, as expected, the solutions are symmetric about the mean of the PDF and exhibit discontinuities at the membranes as defined in (4.2.3). For finite values of the permeability and for very short diffusion times, the PDF has the appearance of a Gaussian, or segments thereof, and qualitatively fits the function:

$$\rho = \frac{1}{\sqrt{4\pi T}} e^{\frac{-x^2}{4T}}, \tag{5.1.1}$$

where T is the reduced diffusion time: $T \equiv Dt/\alpha^2$. However, as we increase the diffusion time, the solution loses its similarity with a Gaussian. This effect is produced by the presence of the barriers which makes the domain not homogenous. In fact, as we saw in Section 2.3.2, for a bounded domain, the Green's function for the diffusion equation, when the initial condition is a Dirac Delta function, has a much more complicated form than a Gaussian.

The results are broadly similar to those presented in [31]: the solutions look similar but have different characteristics in accordance with the values of permeability adopted in the simulations. As shown in Figure ??, for reduced permeability $P = 2.0$ and for a very short diffusion time, $T = 0.1$, the shape of the solution looks very similar to a Gaussian distribution with discontinuities. As the diffusion time increases, the only maximum in the solution decreases and the height of the jumps have decreased. This agrees with the physics of the diffusion process. For a very long diffusion time $T = 10$, represented by the dark green curve in Figure ??, the solution appears to be almost flat over the whole domain. The analysis for the behaviour of the solution when $P = 0.5$, reported in Figure ??, is very similar to the previous case. However it is worth noting that, for a lower value of membrane permeability, diffusion is slower which is again in accordance with the theory.

Having introduced and verified the shape of the numerical solution $\rho(x, t)$, below we present some tests we perform in order to guarantee trustworthy numerical computations.

5.2 Reliability and Numerical Accuracy of the Simulations

In the previous section, we verified that the solutions behave accordingly to the physics of a diffusion process in an inhomogeneous system. Here, we describe some additional tests that verify the reliability and the numerical accuracy of the code and the results. First, we discuss the choice of domain size. Next we discuss the dependence of the error on the grid size.

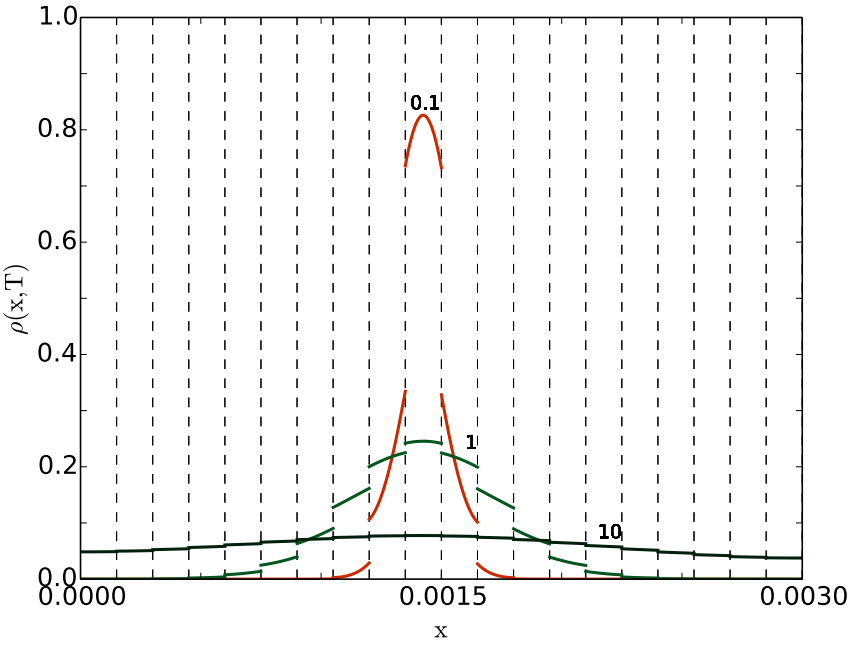

(a) $P = 2.0$

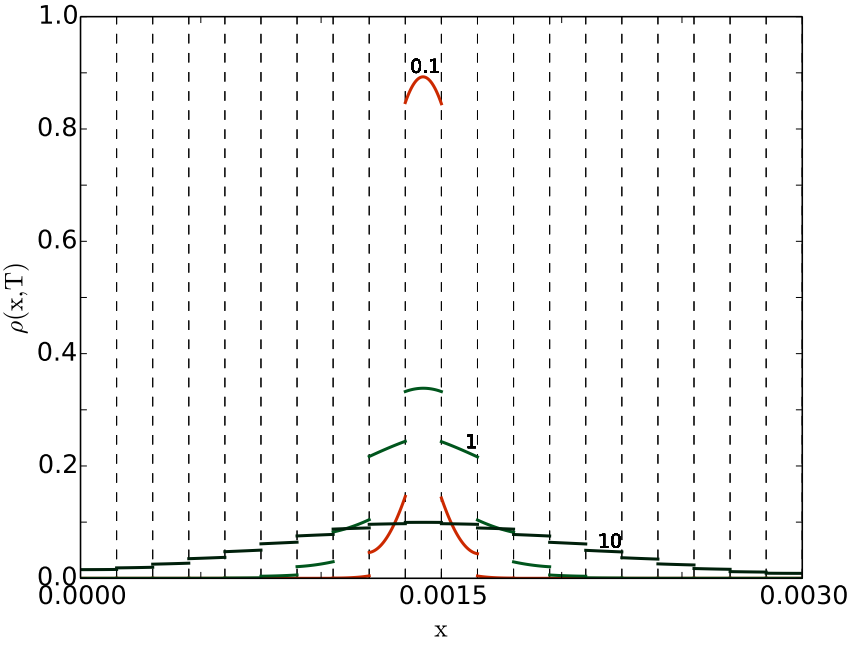

(b) $P = 0.5$

Figure 5.1: Probability density function of diffusing particles from a delta function IC in the middle of a 20 region system at reduced times $T = 0.1,\ 1,\ 10$ as labelled and different reduced permeability P. The dashed lines represent the location of the cellular membranes.

Numerical Simulation Parameters	Value used
Intracellular length l_{in}, μm	15
Extracellular length l_{out}, μm	15
Intracell. diffusion coefficient D_{in}, cm^2/s	0.5e-5
Extracell. diffusion coefficient D_{out}, cm^2/s	0.5e-5
Diffusion time t, msec	18
Permeability p, cm/s	0.5

Table 5.3: Range of parameters used in the numerical simulation to look at the change at the boundaries for the case of equally spaced barriers and same diffusion coefficient.

5.2.1 Truncation of the domain

In Section 4.1 we introduce our model as an infinite system of regions of alternating intracellular and extracellular space. For obvious computational reasons, it is necessary to truncate the domain and define conditions (4.2.2) at the boundaries of the domain. In this section we discuss the choice of domain size, i.e., the number of regions over which the diffusion is simulated. An appropriate choice may be a domain for which the change of $\rho(x,t)$ at the boundaries is considered small enough so that the solutions approximate those for which the domain is infinite.

Here, we present the behaviour of the DPDF boundaries of the computational domain for two different systems. In the first, the domain is a set of regions with the same width and same diffusion coefficient. The permeability of the membranes is $p = 0.5$cm/s and the diffusion time is $t = 18$ms. In the second case, we distinguish the extracellular and intracellular regions by varying the width of the alternating regions, and choosing different diffusion coefficients for the two regions. For this second experiment, the permeability of the barriers is $p = 0.01$cm/s and the diffusion time is $t = 30$ms. In both cases, we considered the same number of regions, $N = 20$, each discretized in a set of 40 grid points ($nx = 40$). The values of all the parameters used in the experiments are reported in Tables 5.3 and 5.4, respectively. It is important to mention that the chosen diffusion times are considered to be long enough to simulate a DW-MRI experiment [13] [4]. In Figure 5.2, the change at the extreme boundaries of the domain are shown for the first simulation. Because the source of diffusing particles

Numerical Simulation Parameters	Value used
Intracellular length l_{in}, μm	24
Extracellular length l_{out}, μm	6
Intracell. diffusion coefficient D_{in}, cm^2/s	1e-5
Extracell. diffusion coefficient D_{out}, cm^2/s	2.5e-5
Diffusion time t, msec	30
Permeability p, cm/s	0.001

Table 5.4: Range of parameters used in the numerical simulation to look at the change at the boundaries for the case of not equally spaced barriers and different diffusion coefficient for the intracellular and extracellular regions.

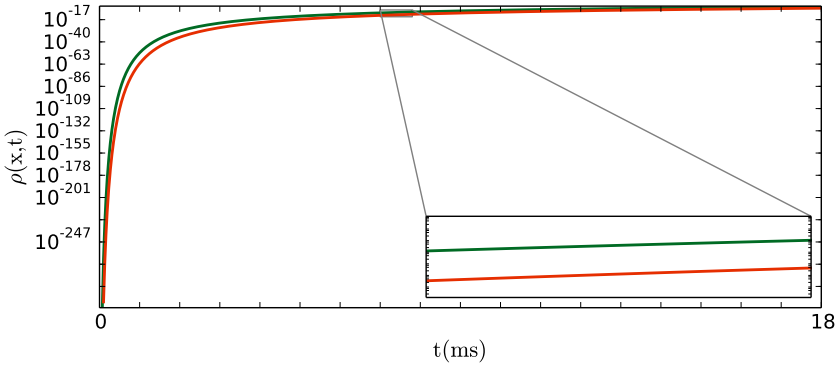

Figure 5.2: Change at the very left (orange) and right (green) points of the discretized domain for a system with equally spaced barriers and constant diffusion coefficients after a diffusion time $t = 18$ms.

is at the centre of the discretized domain, the changes at the left (orange) and right (green) grid points are very similar for the entire duration of the experiment. For very short diffusion times the changes are extremely small and, even though seem to increase rapidly for slighter longer times, they do not seem to be growing exceedingly fast. This behaviour is in accordance with the physics of the diffusion process. Even though the diffusion time for this experiment is shorter than the ones normally used in a DW-MRI experiment, we concluded that the change at the boundary is still negligible and, therefore, our choice of domain size is appropriate. In Figure 5.3 the change at the boundaries for a domain with parameters as described in Table 5.4 is shown. For this experiment we choose a value for the permeability that is more physiologically relevant for cellular membranes [13] and a diffusion time that is typical

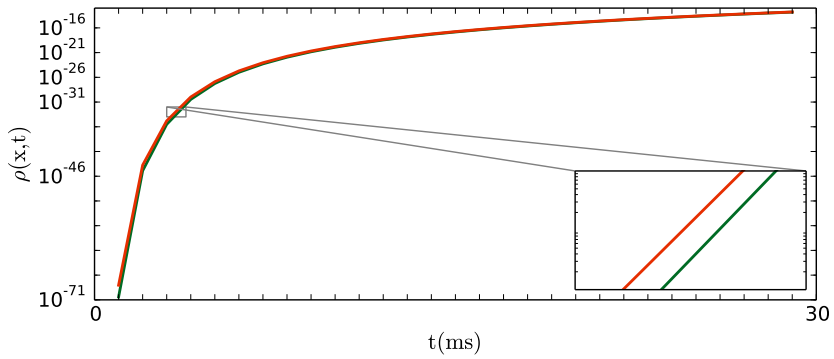

Figure 5.3: Change at the very left (orange) and right (green) points of the discretized domain for a system with not equally spaced barriers and different diffusion coefficients for intracellular and extracellular regions after a diffusion time $t = 30$ms.

of a DW-MRI experiment. The analysis of the results reported in Figure 5.3 is very similar to that of the first experiment. However, it is worth mentioning that, even though the diffusion coefficient is larger for both the intracellular and extracellular regions than in the previous experiment, the fact that the permeability p is much lower in this case ensures the change at the boundaries remains negligible even for longer diffusion times.

After this analysis, we can conclude that the domain of computation we choose (20 alternating regions each discretized into 40 grid points) is big enough to assume that the effects of computing on a finite domain are negligible. Theoretically, we could have chosen to work with a finer grid than the one considered here, but this would have led to much larger computations.

5.2.2 Numerical accuracy

In this part, we present some additional tests of the numerical approximations. As we explained in Section 4.3, we use a second-order centred finite-different scheme to discretize in space the diffusion equation for our problem (4.2.1). In the case of a diffusion problem solved by using a second-order finite-difference scheme, we would expect a rate of convergence proportional to Δx^2, where Δx is the grid spacing [21]. Thus far we have considered grids for which each region of intracellular and

Points per region	Total points in the domain	Δx
160 (reference grid)	3200	9.375e-7
80	1600	1.875e-6
40	800	3.75e-6
20	400	7.5e-6
10	200	1.5e-5

Table 5.5: Number of grid points used in the simulations in order to estimate the error. The finest one is used as reference for estimates on coarse grids.

extracellular space is discretized using $nx = 40$ points. Here, we estimate the rate of convergence for the error for numerical solutions on coarser-grids in comparison to a fine grid solution considered as reference.

Because we are dealing with a inhomogenous domain, finding the exact analytical solution requires a very involved mathematical calculation (see Section 2.3.2). Therefore, we obtain an estimate of the error for the problem by computing the solution on a very fine grid, say with grid spacing $\overline{\Delta x}$, and use this as a reference solution for computing errors on some sequence of coarser grids. A summary of the number of grid points used in each run with the relative Δx is reported in Table 5.5. In order to compare the approximate solution $u^{\Delta x}$ corresponding to one of the coarser grids with the approximation $u^{\overline{\Delta x}}$ on the fine grid, we need to make sure that these two grids contain coincident grid points at which we can directly compare the solutions. It is typical to choose the grids in such a way that all the grid points on the coarser grid are also on the fine grid [21]. In order to give an estimate of the rate of convergence of the error, let $\bar{u}^{\Delta x}$ be the restriction of the fine-grid solution to the Δx-grid, so that we can define the approximate error $\bar{E}(\Delta x) = ||u^{\Delta x} - \bar{u}^{\Delta x}||$, analogous to the true error $E(\Delta x) = ||u^{\Delta x} - \hat{u}^{\Delta x}||$ [21]. Given this definition we can write

$$u^{\Delta x} - \bar{u}^{\Delta x} = (u^{\Delta x} - \hat{u}^{\Delta x}) + (\hat{u}^{\Delta x} - \bar{u}^{\Delta x}). \tag{5.2.1}$$

We have already stated that the method we use to discretize the diffusion equation is supposed to be second-order accurate ($p = 2$), and we know also that $\overline{\Delta x}^2 \ll \Delta x^2$. From this last information we can conclude that the second term on the right hand side of (5.2.1), the true error on the $\overline{\Delta x}$-grid, should be negligible compared to the

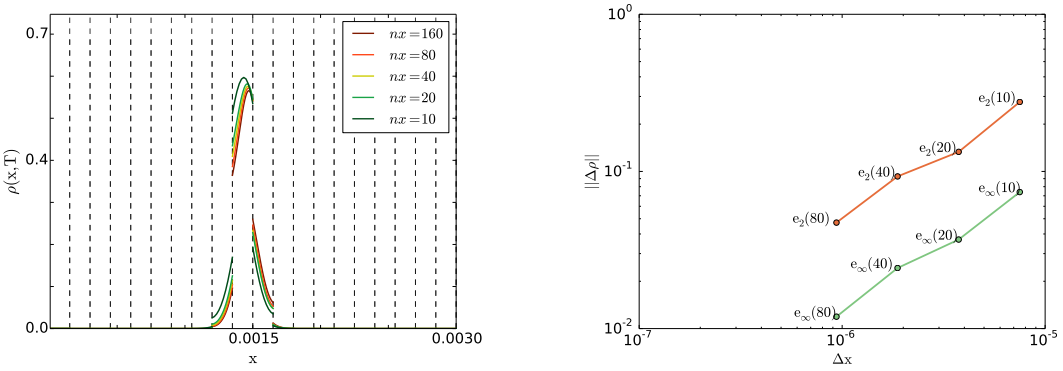

(a) (b)

Figure 5.4: 5.4a: coarser grid solution compared to a fine one as labelled. The domain is a system of 20 regions with equal spacing and permeability $p = 0.5$. The diffusion coefficient is constant across the different regions and the diffusion time is $t = 15$ms. 5.4b: 2-norm (orange) and ∞-norm (green) of the error for coarser-grid solution in comparison to a very fine one as labelled.

first one, the true error on the Δx-grid, and, therefore $\bar{E}(\Delta x)$ should give an accurate estimate of the error. In particular, because the discretization is second-order accurate we may expect

$$E(\Delta x) = C\Delta x^2 + o(\Delta x^2) \quad \Delta x \to 0. \tag{5.2.2}$$

In particular, if Δx is sufficiently small then we can just write: $E(\Delta x) \approx C\Delta x^2$. Suppose now, that we decide to refine the grid by a factor of 2, say. Then we expect

$$E(\Delta x/2) \approx C(\Delta x/2)^2. \tag{5.2.3}$$

Defining the error ratio to be

$$R(\Delta x) = \frac{E(\Delta x)}{E(\Delta x/2)}, \tag{5.2.4}$$

and given the previous analysis, we can write

$$R(\Delta x) \approx 2^p. \tag{5.2.5}$$

This, for the standard diffusion problem discretized on a uniform grid, we would get a $\mathcal{O}(\Delta x^2)$ convergence assuming that the diffusion coefficient is constant and that the functions describing the source terms and boundary conditions are smooth.

In Figure 5.4 we present results obtained at various grid spacing. Plots of the

solution with fine- and coarser-grids are reported in Figure 5.4a. The initial condition is chosen to be the same for each run, the membranes are equally spaced across the domain, the diffusion coefficient is taken as constant in both the extracellular and intracellular space, and the diffusion time is $t = 15$ms. In Figure 5.4b we present the computation of the 2-norm (orange) and ∞-norm (green) of the error of the solution on coarser grids using, as reference, a fine grid with $nx = 160$ points per region. It is easy to notice that, on a log-log plot as in Figure 5.4b, the rate of convergence seems to be $\mathcal{O}(\Delta x)$ rather than $\mathcal{O}(\Delta x^2)$ as we would expect. We justify this behaviour by noticing that, for this problem, we do not have the smoothness required for a second-order convergence as there are discontinuities across the distinct regions as defined in (4.2.3). Hence, the requirements that lead to second-order convergence in Δx do not apply. Our solution has discontinuities at the cellular membranes and therefore are not smooth. Usually, in order to maintain a good order of convergence in the presence of jumps, it is good practice to locate the discontinuity and place a mesh point as close to it as possible [5]. However, in this case, we discretize (4.2.3) in a way such that two different values of $\rho(x, t)$ are associated with each interface. This way of treating the discontinues affected, in fact, the order of convergence of the solution giving a rate proportional to $\mathcal{O}(\Delta x)$.

Now that we have seen what the solution looks like for a toy problem, in the next section, we will define a domain that is supposed to model more realistically a system of cells in human tissue.

5.3 Computing the Probability Density Function

In the previous section, we have verified the reliability and the numerical accuracy of the code. In this section we compute the solution for a system very similar to the one presented in Section 5.1. The main difference lies in the choice of the parameters. As explained in Section 2.1, in the human body there are cells with different shapes and sizes depending on their function. Here we will present the computations for the DPDF $\rho(x, t)$ for systems of cells arranged on a periodic lattice (see Section 4.1) for various values of key membrane parameters and for various sizes of intracellular and

Numerical Simulation Parameters	Value used
Number of regions, N	20
Number of grid point for each region, nx	40
Diffusion time, t, ms	50
Time step, Δt	1e-9
Number of time steps, nT	5e10

Table 5.6: Range of parameters used in the numerical simulation to simulate a systems of cells arranged on a periodic lattice with physically relevant parameters.

extracellular space.

Given the results obtained in Section 5.2.1, we choose $N = 20$ alternating regions of intracellular and extracellular space. Independent of the width of each region, we discretize each of them using $nx = 40$ points. We choose the diffusion time to be $t = 50$ms. This value is slightly longer than the one commonly used in DW-MRI. This choice is made in part for a purely practical reason; once the code is parallelized using Message Passing Interface (MPI), using diffusion times longer than those typical of a DWI experiment (typical $t = 30$ms) do not result in significantly or challenging computations. Of course we hope to capture more information about the diffusion of particles by increasing the diffusion time (see Section 2.2.2); we will discuss this in more detail in Section 5.4. We choose the time step to be very small, in particular Δt =1e-9ms. This leads to a time stepper with $nT = 5e10$ total time steps. A summary of the computational parameters used for all the experiments is presented in Table 5.6.

Having introduced the computational parameters, we shall now define the values of the physiological variables involved in the simulations. Because the cells are arranged on a periodic lattice separated by extracellular space, we define the lattice constant to be that portion of the domain which includes one full intracellular region and one full extracellular region. Henceforth, we will denote the lattice constant to be α. We run experiments for three different lattice constants: $\alpha = 3\mu$m, $\alpha = 5\mu$m and $\alpha = 7\mu$m. Moreover, we vary the volume ratio f of intracellular and extracellular space; for every value of α we use $f = 0.8$ and $f = 0.66$. We do not change the values of the diffusion

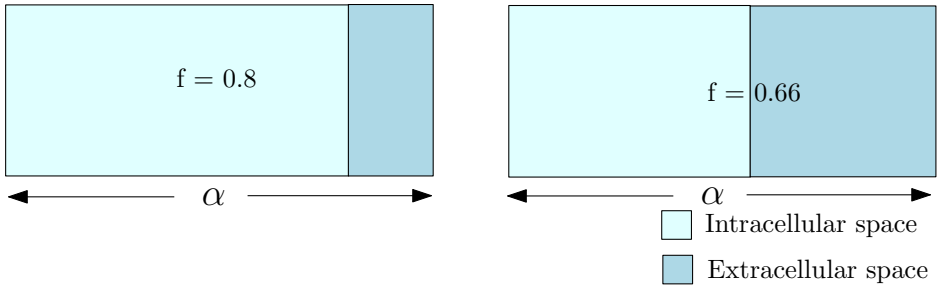

Figure 5.5: Cartoon of the lattice unit used in our system. On the left the volume ratio is equal to 0.8, on the right is 0.66: this structural difference leads to changes in the solution as the regions have different diffusion coefficients.

$\alpha = 3\mu$m			$\alpha = 5\mu$m			$\alpha = 7\mu$m		
	f = 0.8	f = 0.66		f = 0.8	f = 0.66		f = 0.8	f = 0.66
l_{in}	2.4μm	2μm	l_{in}	4μm	1μm	l_{in}	5.6μm	1.4μm
l_{out}	0.6μm	1μm	l_{out}	3.3μm	1.7μm	l_{out}	4.6μm	2.4μm
(a)			(b)			(c)		

Table 5.7: Summary of the width of the intracellular, l_{in}, and extracellular l_{out}, width of the regions in the domain for different values of the lattice constant α and for different volume ratio t.

coefficients for the intracellular and extracellular space in all the simulations, while the permeability of the membranes is changed over a wider variety of cases. The choice for these parameters is dictated by the literature [12] [13] . A summary of the values used is reported in Tables 5.7 and 5.8

Some examples of the solution for different lattice constants and volume ratio are presented in Figures 5.6 - 5.8. In all the cases, the numerical solutions exhibit the same characteristic; in particular, they all have a single maximum that decreases monotonically towards the extremes of the domain. It can be seen that, due to the

Numerical Simulation Parameters	Value used
Intracell. diffusion coefficient D_{in}, cm^2/s	1e-5
Extracell. diffusion coefficient D_{out}, cm^2/s	2.5e-5
Diffusion time t, msec	50
Permeability p, cm/s	0.01- 0.05 - 0.1

Table 5.8: Physiological parameters used to model the cellular domain.

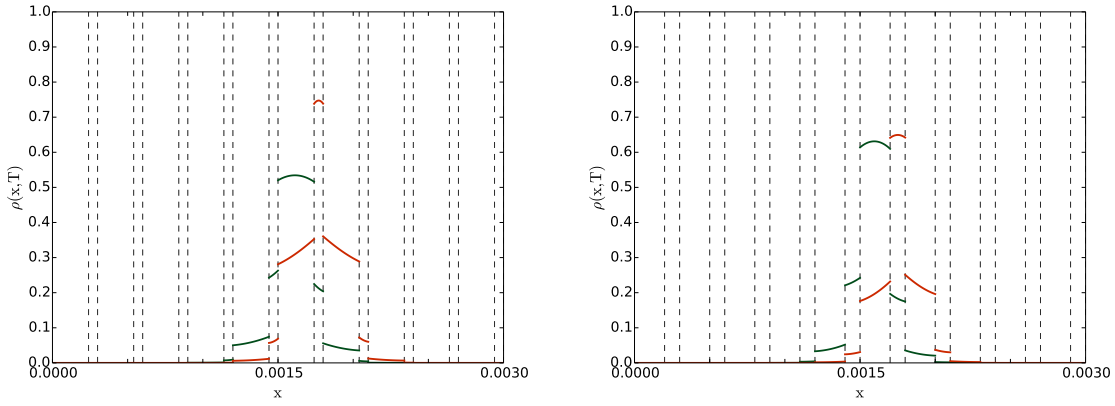

(a) (b)

Figure 5.6: Numerical solutions for a system of cell with lattice constant $\alpha = 3\mu$m and volume ratio $f = 0.8$ (5.6a) and $f = 0.66$ (5.6b). In both cases, the green lines represent a solution with a delta function IC centred within an intercellular region, while the orange lines represents a solution with a delta function IC centred inside an extracellular region. The dashed lines represents the positions of the cellular membranes.

presence of barriers, all the curves are discontinuous with jumps at each membrane (whose locations are represented by dashed lines) and $\rho(x,t)$ is clearly not a Gaussian. If the ICs are not centred in the middle of the domain, then the symmetry is lost. This follows from the fact that the displacement that each particle experiences depends on how far is it from a semi-permeable membrane as well as the permeability of the membrane and the diffusion coefficient.

A note on the MPI computation

In this section, we discuss the parallelizations of the source code using Message Passing Interface-MPI. Before providing more insight on this, it is important to remember that we define the domain as a periodic lattice. Each lattice unit is discretized in the same way, except for the ones on the very left and right (where we have Neumann boundary conditions to consider). In Section 5.2.1, we choose a large enough number of layers across the domain to ensure that the value of the probability density function is negligible in the outermost layers at the longest diffusion times; we have discussed the validity of this assumption in Section 5.2.1. For the computation of the ADC, because

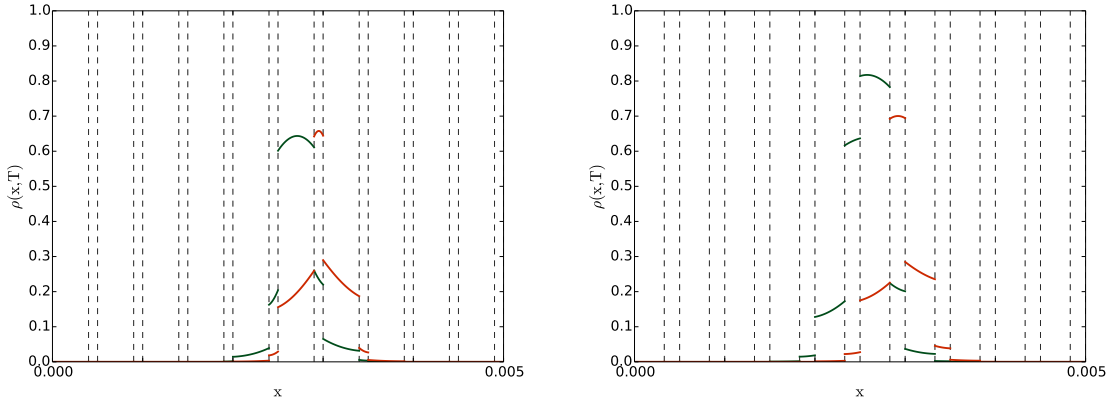

(a) (b)

Figure 5.7: Numerical solutions for a system of cell with lattice constant $\alpha = 5\mu$m and volume ratio $f = 0.8$ (5.7a) and $f = 0.66$ (5.7b). In both cases, the green lines represent a solution with a delta function IC centred within an intercellular region, while the orange lines represents a solution with a delta function IC centred inside an extracellular region. The dashed lines represents the positions of the cellular membranes.

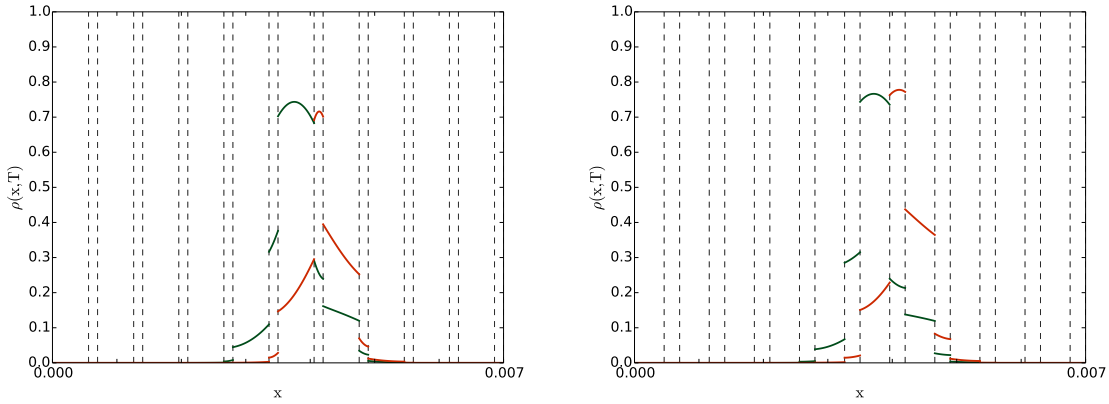

(a) (b)

Figure 5.8: Numerical solutions for a system of cell with lattice constant $\alpha = 7\mu$m and volume ratio $f = 0.8$ (5.8a) and $f = 0.66$ (5.8b). In both cases, the green lines represent a solution with a delta function IC centred within an intercellular region, while the orange lines represents a solution with a delta function IC centred inside an extracellular region. The dashed lines represents the positions of the cellular membranes.

the system is periodic and has translational symmetry, it is only necessary to compute the solutions $\rho(\zeta_0|x,t)$ for values of ζ_0 over the single lattice unit located in the middle of the domain (see Section 5.3 for discussion). Thus we need only to compute $\rho(\zeta_0,x,t)$ with a delta function initial condition to be centred at each of the grid points within the lattice unit, i.e., for ζ_0 taken at each grid point with the lattice unit. Because we are considering $nx = 40$ points per region, this means we are required to run 80 jobs (40 for the intracellular space, and 40 for the extracellular space) serially for the desired diffusion time. To improve the efficiency of the code and be to able to have as much data as possible we have parallelized the code using the Python library mpi4py. In particular, we compute the solution corresponding to each point ζ_0 is the lattice unit simultaneously using 80 processors on the supercomputer Saw, part of the Shared Hierarchical Academic Research Computing NETwork (SHARCNET) consortium.

5.4 Computing the ADC

In this section, we recall the notion of Apparent Diffusion Coefficient which has beed introduced in Section 3.2 and we present the results obtained from using different approaches. The ADC is a measure of the constrained diffusion that water molecules experience while diffusing in an inhomogenous medium and, theoretically, it is possible, from its value, to infer information about the tissue structure and integrity [29].

In the first part of this section, we will compute the ADC from the definition derived in Section 3.2.2. We will refer to this value of the apparent diffusion coefficient using the notation $D^{(2)}_{\text{ADC}}$: this will help us keep in mind that this represents the value of the ADC computed from the signal by expanding the cosine term in (3.1.1) in Taylor series up to *second* order. We will compare this measurement for the ADC with others obtained by averaging the second moment of the DPDF as in Section 5.4.2. From now on, we will refer to the ADC computed using this procedure as D_{AVE}. In the last part, we will present results for the ADC we obtain by expanding the cosine term in the signal up to the *fourth* order. We will distinguish this value of the ADC using the notation $D^{(4)}_{\text{ADC}}$.

5.4.1 ADC from the signal - 2^{nd} moment

In Section 3.2.2, we introduce and derive a formula (3.2.16) However, before being able to use this formula, we must derive the signal value associated with the simulations. That is, having computed the DPDF $\rho(\zeta_0|x,t)$ within a single lattice unit of our domain, (see Section 5.3), we can derive the value for the signal $R(t)$ from (3.1.1). Once we have the value for the signal, we can directly compute the ADC from (3.2.16).

We recall that the signal can be computed from the DPDF via

$$R(\Delta) = \frac{1}{L[\Omega]} \int_{\Omega^-}^{\Omega^+} \int_{\Omega^-}^{\Omega^+} \rho(\zeta_0|x,\Delta) \cos[q(x-\zeta_0)] dx d\zeta_0, \tag{5.4.1}$$

if L is the length of the whole sample Ω. Because of the periodicity of the lattice, we only need to integrate over a single lattice unit, i.e., we can evaluate the outer integral from 0 to α, if α is the lattice unit. We are integrating the inner integral over x, that is, over the entire domain. If χ is the length of the computational domain, then we can say that the inner integral is evaluated from 0 to χ. We justify this simplification because, as discussed in section 5.2.1, $\rho(x,t)$ is small outside this interval, and, therefore, would contribute little to the value of R. Therefore, we can rewrite (5.4.1) as

$$R(\Delta) = \frac{1}{\alpha} \int_{0}^{\alpha} \int_{0}^{\chi} \rho(\zeta_0|x,\Delta) \cos[q(x-\zeta_0)] dx d\zeta_0. \tag{5.4.2}$$

Before evaluating the integral we need to choose a suitable value for q. As explained in Section 3.1.2, q provides the relationship between relative position and phase of the spins, and thus, is related to the distance travelled by the molecules and the associated signal loss. In order to ensure that the signal loss does not decrease as the molecule moves further, we can set the phase change from one side of the domain to the other to be 2π. Thus, given the units of q in Section 3.1.2, we can choose to compute q in the following way

$$q = \frac{\omega}{\chi} = \frac{2\pi}{\chi}, \tag{5.4.3}$$

i.e., over the whole length of the domain the spins experience a complete revolution ω equal to 2π. We summarize the values of q for the chosen domain sizes in Table 5.9.

The double integral is evaluated by using a two-dimensional trapezoidal rule over rectangular regions. The weights in the grid of computation are chosen according

	$\chi = 30\mu$m	$\chi = 50\mu$m	$\chi = 70\mu$m
q	210	125	90

Table 5.9: Values of the q factor used in computing the ADC for different sizes of domain. The choice is made trying to guarantee the maximum proton rephasing during the chosen diffusion time over the entire domain.

to the mesh points spacing; in fact, we recall that we use a different grid spacing for intracellular and extracellular regions. With the simulated signal measured from 5.4.2, the ADC can be computed from

$$D^{(2)}_{\text{ADC}} = -\frac{\log(R(\Delta))}{q^2\Delta}, \tag{5.4.4}$$

where Δ is the chosen diffusion time for the simulation. Plots of the apparent diffusion coefficients, computed in this way, are reported in Figure 5.9.

When $\alpha = 3\mu$m and the volume fraction is f= 0.8 (see Figure 5.9a), for small permeability of the membranes, the ADC seems to decrease quickly in the first part of the diffusion process until it relaxes reaching a constant value. For higher values of permeability (dark green curves), the ADC does not seem to approach any constant value in the chosen time of diffusion. This might by due to the fact that having membranes with higher permeability is equivalent to having increased motility of the molecules of water. It was not practical, given the time of the computation, to increase the diffusion time sufficiently to capture a relaxing value for the ADC in this system.

In Figure 5.9b the ADC spans a smaller range of values. This might be the result of having a smaller volume ratio (i.e., the extracellular space is larger). Bearing in mind that in the extracellular regions the diffusion coefficient is higher, we justify the behaviour of the ADC by saying that in this case the molecules encounter less constraints in the diffusion. This justifies as well the fact that, for lower values of the permeability, the ADC seems to reach a steady value in a shorter time. Similar results were obtained for other cellular configurations (i.e., for different values of lattice constant α and volume fraction f).

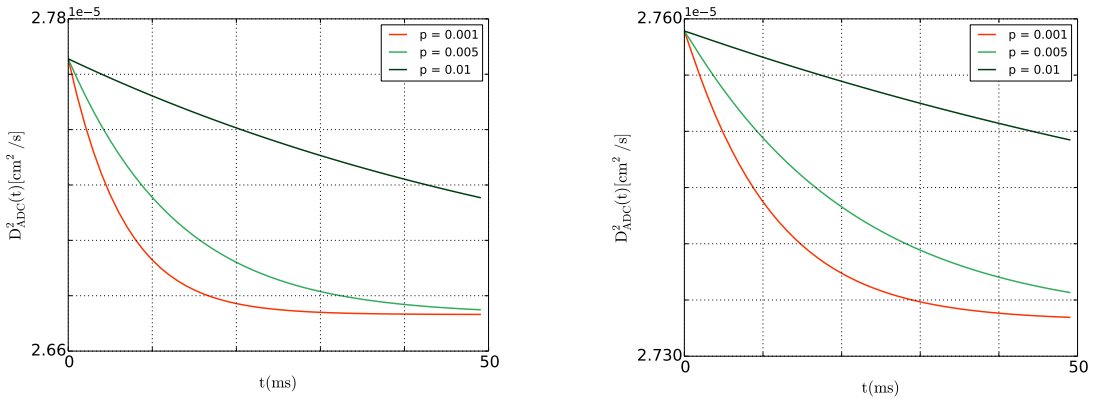

(a) (b)

Figure 5.9: Numerical value $D^{(2)}_{\text{ADC}}$ of the Apparent Diffusion Coefficient computed from the simulated signal by expanding the cosine term up to the second moment. 5.9a corresponds to a system with lattice constant $\alpha = 3\mu$m and $f = 0.8$. 5.9b corresponds to system with $\alpha = 5\mu$m volume fraction $f = 0.66$. The computations are done for different values of permeability, as displayed in the legends.

	$\chi = 30\mu$m	$\chi = 50\mu$m	$\chi = 70\mu$m
q	4.7e-4	7.9e-4	1.1e-4

Table 5.10: Values of the q factor used in computing the ADC for different sizes of domain. This parameters are much smaller than the ones presented in 5.9.

A note about the value of q

At this point, it is worth mentioning something about the changes affecting the behaviour of the $D^{(2)}_{\text{ADC}}$ as computed from the second order expansion of the signal. In particular, we notice that changes in the q value are reflected in qualitative and quantitative changes in the value of the ADC.

We have also computed $D^{(2)}_{\text{ADC}}$ using the same approach used in this section, but for much smaller values of q than the ones reported in Table 5.9. These new values of q are summarized in Table 5.10. Results for $D^{(2)}_{\text{ADC}}$ computed with the updated values of q are presented in Figure 5.10. To make the comparison more meaningful, in Figure 5.10 we report the values of $D^{(2)}_{\text{ADC}}$ for the same volume fractions and lattice constant α as in Figure 5.9. It is easy to notice that, changes in the values of q, do

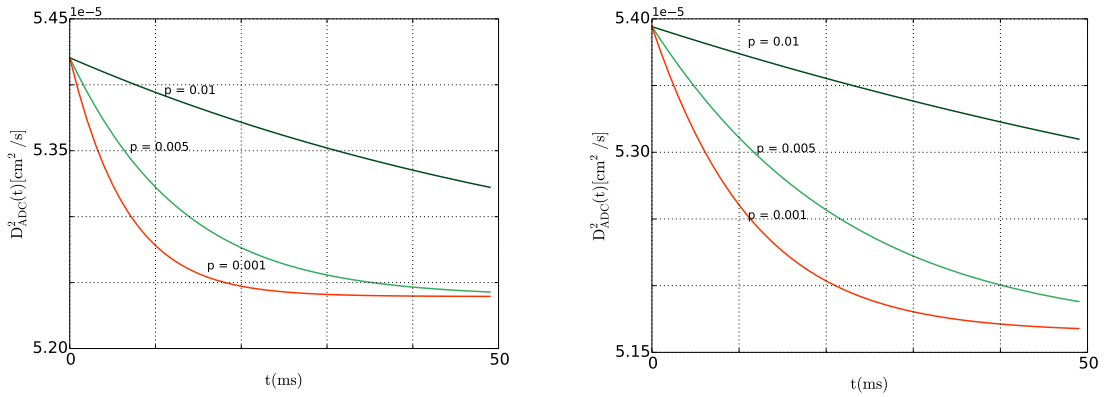

(a) (b)

Figure 5.10: Apparent Diffusion Coefficient computed from the simulated signal by expanding the cosine term up to the second moment in a system with volume fraction $f = 0.8$ and lattice constant $\alpha = 3\mu$m (5.10a) and $\alpha = 5\mu$m (5.10b) and small values of q.

not significantly affect the qualitative behaviour of the apparent diffusion coefficient. However, it is interesting to notice the quantitative changes: for high values of q (see Table 5.9 and Figure 5.9), $D^{(2)}_{\text{ADC}}$ covers a range of parameters between 2.73e-5cm^2/s and 2.76e-5cm^2/s. For small values of q (see Table 5.10 and Figure 5.10), $D^{(2)}_{\text{ADC}}$ spans a wide range of higher values.

We interpret this as an indicator of the fact that the value of q might be choose in an arbitrary way. In fact, changes of an order of magnitude of q seems not to affect the qualitative behaviour of $D^{(2)}_{\text{ADC}}$. Moreover, we believe that quantitative changes in $D^{(2)}_{\text{ADC}}$ due to changes in q indicate that the $\mathcal{O}(q^4)$ terms that are neglected in (3.2.13) are likely not negligible for reasonable values of q, resulting in values of the ADC which are not quantitatively accurate.

We will now compute the ADC as we defined it in Section 4.7 and compare the results.

5.4.2 Averaged ADC

In Section 4.7 we define an ADC by following the analogy with the diffusion relation proposed by Einstein [31]. In particular, we recall that the ADC can be defined by

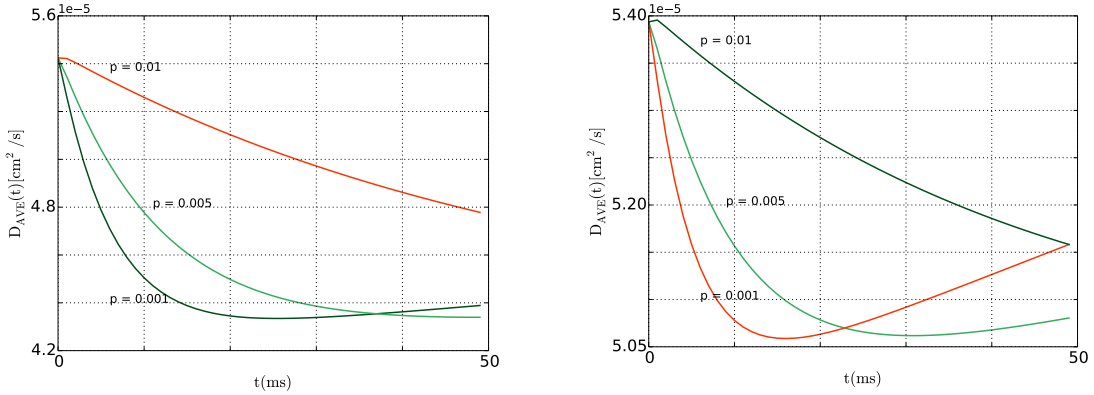

(a) (b)

Figure 5.11: Numerical value of the Apparent Diffusion Coefficient D_{AVE} computed by averaging the second order moment of the solution over a single lattice unit with $\alpha = 3\mu$m. We used different values of membrane permeability, as labelled. 5.11a corresponds to a system with a volume ratio $f = 0.8$ and 5.11b corresponds to a volume ratio $f = 0.66$

averaging the second moment of the displacement probability density function over a single lattice unit

$$D_{\text{AVE}} = \frac{1}{2\Delta\alpha}\int_0^{\alpha}\int_0^{\chi}(x-\zeta_0)^2\rho(\zeta_0|x,\Delta)dxd\zeta_0, \tag{5.4.5}$$

where Δ is the diffusion time. In order to evaluate the integral, we take advantage of the translational symmetry of the solution across our domain. In particular, the contribution to the integral from each lattice unit will be the same. Because of this, we can average the integral over the lattice unit α rather than the whole domain. Thus, we are required to compute all the solutions corresponding to ICs centred at the grid points inside a lattice unit. The computation of the ADC in this case is more straightforward than the one presented in Section 5.4.1 as there is no need to compute the signal. The results are reported in Figures 5.11-5.13.

For low permeability of the membranes, D_{AVE} appears to decrease rapidly initially, then eventually less so. However, rather than relaxing to a constant value, when the lattice unit is small ($\alpha \leq 5\mu$m) and the permeability is $p = 0.001$, the D_{AVE} reaches a minimum and eventually starts increasing. This behaviour is clear in Figures 5.11a, 5.11b and 5.12b, but we expect the same to happen in cellular configurations where

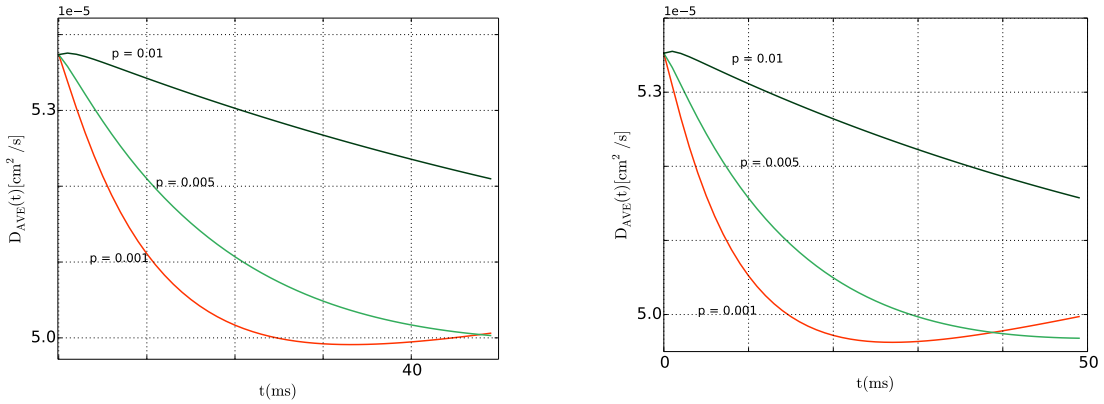

(a) (b)

Figure 5.12: Numerical value of the Apparent Diffusion Coefficient D_{AVE} computed by averaging the second order moment of the solution over a single lattice unit with $\alpha = 5\mu$m. We used different values of membrane permeability, as labelled. 5.12a corresponds to a system with a volume ratio $f = 0.8$ and 5.12b correspond to a volume ratio $f = 0.66$

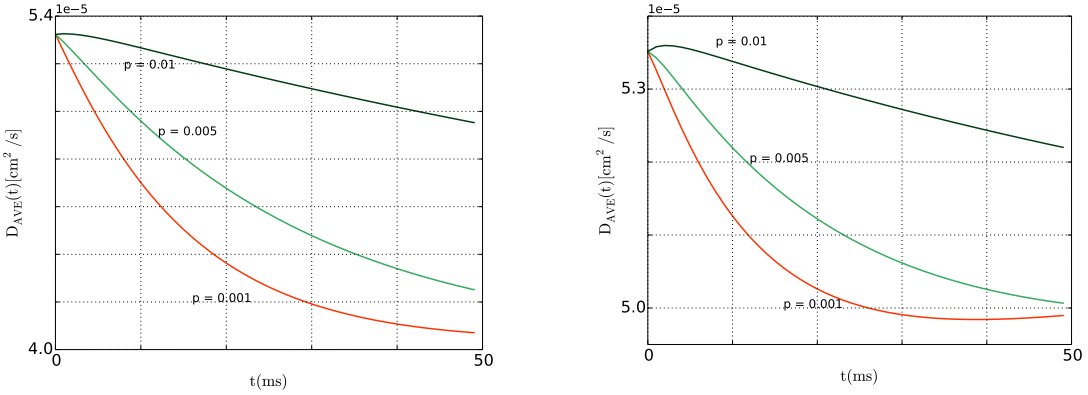

(a) (b)

Figure 5.13: Numerical value of the Apparent Diffusion Coefficient D_{AVE} computed by averaging the second order moment of the solution over a single lattice unit with $\alpha = 7\mu$m. We used different values of membrane permeability, as labelled. 5.13a corresponds to a system with a volume ratio f= 0.8 and 5.13b correspond to a volume ratio f = 0.66

α	$f = 0.8$	$f = 0.66$
3 μm	23 ms	13 ms
5 μm	> 50 ms	27 ms
7 μm	> 50 ms	> 50 ms

Table 5.11: The point where the minimum for D_{AVE} occurs for very low permeability depends on the lattice constant and on the volume fraction of intracellular and extracellular space.

the volume ratio f is smaller and the diffusion time is longer. The point where the minimun of D_{AVE} occurs seems to depend strongly on the structure of the domain, the size of the lattice unit, and on the value of the permeability of the cells. In particular, the minimum appears to shift to higher diffusion times as we increase the size of the lattice and the volume fraction. A summary of the value when the minimum occurs in each case is reported in Table 5.11.

This behaviour of D_{AVE} is associated with its definition: in fact, in Section 4.7, we make use of the relation for the diffusion coefficient for the case of homogenous medium to derive the expression for D_{AVE} used in this section. When the permeability is very small, the molecules encounter more difficulties in passing the barriers. In fact, in the presence of these barriers, for long diffusion times, some particles diffuse very slowly and eventually are reflected when they encounter a barrier. The point where the minimum occurs depends on the structure of the lattice (volume fraction) as well as the size of the regions: when the volume fraction is lower, then we have more extracellular space that has a higher diffusion coefficient. This might influence the behaviour of the apparent diffusion coefficient as the particles move faster in these regions.

For higher values of permeability, given the diffusion time for which we performed the simulation, we do not notice any increase in the value of D_{AVE}. We justify this by saying that, when the permeability is higher, then particles encounter less resistance at the membranes and move more easily.

The important point of this section is that, given these results, we believe that it is possible to extract information about the structure of the tissue and the size of

the cells from the value and the behaviour of the apparent diffusion coefficient. To support this hypothesis we will compute the ADC from the simulated signal including higher order terms in the approximation and then compare the results with the one just presented.

5.4.3 ADC from the signal - 4^{th} moment

In Section 5.4.1 and 5.4.2 we present various results for the apparent diffusion coefficient. Although we could notice that the two different approaches have a similar qualitative behaviour, we could notice as well differences especially in the case of small cell sizes.

The ADC presented in this section is computed using a simple mathematical approach; we want to extend the approach of Section 3.2.2 by considering a higher order term in the Taylor expansion.

The important point here is that the formula that has been used so far in the literature is based on the assumption of homogeneous domain: as we explained in Section 2.1, this premise is not supported in the case of diffusion in human tissue. Moreover, truncating the Taylor expansion at the second order might suppress some precious information about the structure of the tissue we are analyzing.

As in Section 5.4.1, to calculate the ADC, we need to simulate the signal via (see Section 3.3.1)

$$\log(R(\Delta)) = -\frac{1}{L(\Omega)}\int_{\Omega^-}^{\Omega^+}\int_{\Omega^-}^{\Omega^+}\rho(\zeta_0|x,\Delta)q^2\frac{(x-\zeta_0)^2}{2!}dxd\zeta_0 + \frac{1}{L(\Omega)}\int_{\Omega^-}^{\Omega^+}\int_{\Omega^-}^{\Omega^+}\rho(\zeta_0|x,\Delta)q^4\frac{(x-\zeta_0)^4}{4!}dxd\zeta_0 + \mathcal{O}(q^2+q^4)^2. \tag{5.4.6}$$

For the integral to converge, we truncate the domain using the same approach of Section 5.4.1. We choose the value for q following the same hypothesis as in Section 5.4.1 (see Table 5.9). The signal now can be computed from the following expansion

$$\log(R(\Delta)) = -\frac{1}{\alpha}\int_0^{\alpha}\int_0^{\chi}\rho(\zeta_0|x,\Delta)q^2\frac{(x-\zeta_0)^2}{2!}dxd\zeta_0 + \frac{1}{\alpha}\int_0^{\alpha}\int_0^{\chi}\rho(\zeta_0|x,\Delta)q^4\frac{(x-\zeta_0)^4}{4!}dxd\zeta_0 + \mathcal{O}(q^2+q^4)^2. \tag{5.4.7}$$

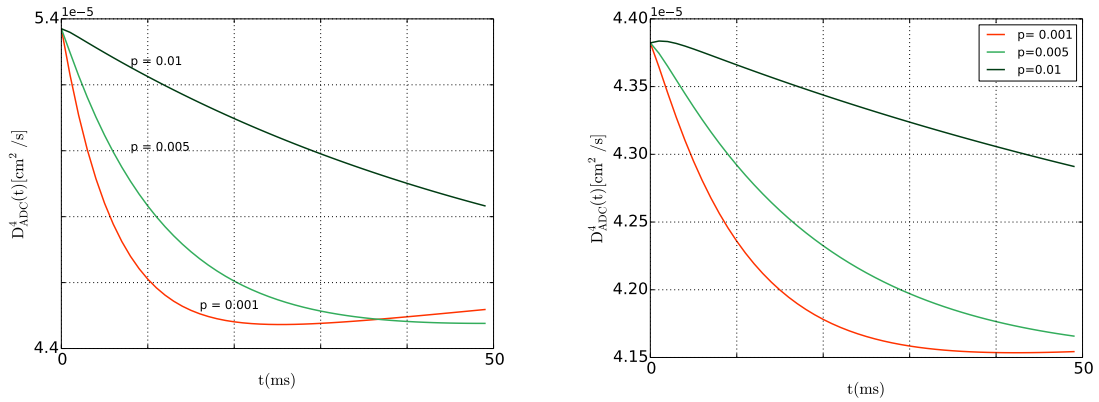

(a) (b)

Figure 5.14: Apparent Diffusion Coefficient $D^{(4)}_{\text{ADC}}$ computed from the simulated signal by expanding the cosine term up to the fourth order for a system with volume fraction $f = 0.8$ and lattice constant $\alpha = 3\mu$m (5.14a) and $\alpha = 5\mu$m (5.14b). Membrane permeability as labelled.

We compute the ADC via

$$D^{(4)}_{\text{ADC}} = -\frac{\log(R(\Delta))}{q^2\Delta}, \tag{5.4.8}$$

where Δ is the diffusion time in the simulation and the superscript 4 indicates that this value of the ADC is the result of a fourth order expansion.

The results are reported in Figures 5.14–5.15. As expected, considering higher order moments in the Taylor expansion of 5.4.1 reveals some features in the value of the ADC that are more similar to those presented in Section 5.4.2. For small membrane permeability and small volume fractions the D^4_{ADC} decreases rapidly for short diffusion times and in the case of small lattice constant $\alpha = 3\mu$m, it has a minimum and increases for longer times t (see Figure 5.14a). This seems justifiable the discussion of Section 5.4.2.

For volume fraction $f = 0.66$ and bigger lattice constants such as $\alpha = 5\mu$m (Figure 5.15a) and $\alpha = 7\mu$m (Figure 5.15b), the behaviour of $D^{(4)}_{\text{ADC}}$ is really similar that of D_{AVE}, but the range of values it seems to cover is smaller and more similar to those of $D^{(2)}_{\text{ADC}}$.

Finally, we can conclude that, when the inhomogeneity of the medium is considered, computing the ADC from the second order expansion of the signal miss some

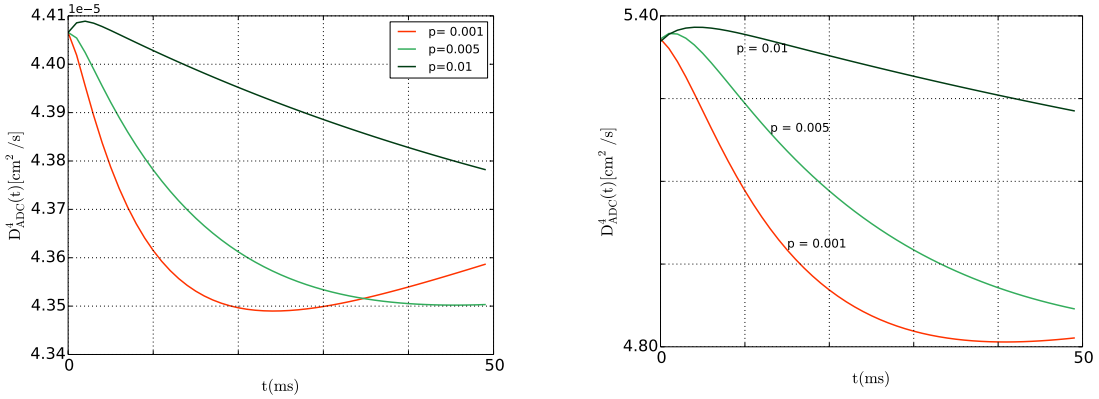

(a) (b)

Figure 5.15: Apparent Diffusion Coefficient $D^{(4)}_{\text{ADC}}$ computed from the simulated signal by expanding the cosine term up to the fourth order for system with volume fraction $f = 0.66$ and lattice constant $\alpha = 5\mu$m (5.15a) and $\alpha = 7\mu$m (5.15b). Membrane permeability as labelled.

information. In the case of having the domain of computation as a periodic lattice, the definition of the ADC as given in Section 4.7 seems efficient. In fact, it requires just the computation of the solution over a single lattice unit to compute an averaged ADC. Results obtained for D_{AVE} agree with the computation of $D^{(4)}_{\text{ADC}}$, i.e., when higher order moments are included.

It is also useful to remind that the computation for D_{AVE} and $D^{(4)}_{\text{ADC}}$ require the computation of the DPDFs, i.e., $\rho(\zeta_0|x,t)$. Therefore, these measurements for the apparent diffusion coefficient cannot be used in practice. However, we believe that the models developed in this study could be used to address questions in diffusion-MRI.

Chapter 6
Conclusions and Future Work

Diffusion Weighted-Magnetic Resonance Imaging (DW-MRI) is a field of great research interest which focuses constantly on improving the accuracy of imaging schemes as well as validating new methodologies. In this thesis, we proposed an idealized model for tissues to simulate diffusion in a non-homogenous media as a possible tool to test, and potentially remove, the hypothesis of homogeneity commonly used in DWI. The model we develop is as easy as it is versatile: different cellular and extracellular space sizes, diffusion coefficients and membrane permeability values can be tuned in the source code in order to produce data for many different configurations.

We validated and tested the results of our model by computing the numerical solution for the Displacement Probability Density Function (DPDF) by using a second-order finite-difference method. The results are broadly similar with the literature [31] and agree with the physics of a diffusion process. Numerical tests for the rate of convergence reveal that our model has less than second-order convergence. This is not unexpected as the computational grid is not discretized uniformly and the model presents discontinuities at the interfaces in the presence of cellular barriers. The main result regarding the shape of the DPDF in a complex medium is that it cannot be approximated as a Gaussian distribution. This was not surprising as the domain considered is not homogenous.

Having numerically computed the shape of the DPDF we are able to measure the Apparent Diffusion Coefficient (ADC) for various cellular configurations. The results for the ADC vary when we do not make the assumption of homogenous medium. In particular, $D^{(2)}_{\mathrm{ADC}}$ and D_{AVE} seem to have very different behaviours when computed for

an inhomogeneous medium. Many of these discrepancies are removed when the ADC is computed from the signal including higher order moments, ($D^{(4)}_{\text{ADC}}$), meaning that much information is lost when truncating the expansion of the signal and considering just the second order moment in the computation of the ADC.

As explained is Sections 4.7 and 5.4.2, a measure for the ADC (D_{AVE}) can be computed directly having the solution $\rho(x,t)$ to the model. Although the results obtained for the ADC using the definition for the D_{AVE} seem to well represent the presence of inhomogeneities in the domain, the application of (4.7.14) is not practical. In fact, the formula in (4.7.14) can be used to compute the ADC in a single voxel provided that we know the numerical solution of $\rho(x,t)$. It would be practical to be able to derive an expression for D_{AVE} that comes directly from the measured DW-MRI signal as defined in (3.1.1). A possible approach might involve measurements of the signal for different values of the q value. Let R_1 and R_2 be the relative echo height measured in standard DW-MRI experiments using different values for the q factor. Therefore, according to (5.4.2), we can write

$$R_1(\Delta) = \frac{1}{\alpha}\int_0^{\alpha}\int_0^{\chi} \rho(\zeta_0|x,\Delta)\cos[q_1(x-\zeta_0)]dxd\zeta_0, \tag{6.0.1}$$

$$R_2(\Delta) = \frac{1}{\alpha}\int_0^{\alpha}\int_0^{\chi} \rho(\zeta_0|x,\Delta)\cos[q_2(x-\zeta_0)]dxd\zeta_0. \tag{6.0.2}$$

We can expand (6.0.1) and (6.0.2) in Taylor series as in Section 3.3.1 to get

$$\begin{aligned} R_1(\Delta) = 1 &- \frac{1}{L(\Omega)}\int_{\Omega^-}^{\Omega^+}\int_{\Omega^-}^{\Omega^+} \rho(x|x_0,\Delta)q_1^2\frac{(x-x_0)^2}{2!}dxdx_0 \\ &+ \frac{1}{L(\Omega)}\int_{\Omega^-}^{\Omega^+}\int_{\Omega^-}^{\Omega^+} \rho(x|x_0,\Delta)q_1^4\frac{(x-x_0)^4}{4!}dxdx_0 + \mathcal{O}(q_1^6(x-x_0)^6), \end{aligned} \tag{6.0.3}$$

and

$$\begin{aligned} R_2(\Delta) = 1 &- \frac{1}{L(\Omega)}\int_{\Omega^-}^{\Omega^+}\int_{\Omega^-}^{\Omega^+} \rho(x|x_0,\Delta)q_2^2\frac{(x-x_0)^2}{2!}dxdx_0 \\ &+ \frac{1}{L(\Omega)}\int_{\Omega^-}^{\Omega^+}\int_{\Omega^-}^{\Omega^+} \rho(x|x_0,\Delta)q_2^4\frac{(x-x_0)^4}{4!}dxdx_0 + \mathcal{O}(q_2^6(x-x_0)^6), \end{aligned} \tag{6.0.4}$$

for R_1 and R_2 respectively. Using the definition (4.7.14) for the D_{AVE}, and (3.3.1) and

(4.7.14) to rewrite the fourth order term, we can rewrite (6.0.3) and (6.0.4) as

$$R_1(\Delta) = 1 - \Delta q_1^2 D_{\text{AVE}} + \frac{1}{6}\Delta q_1^4 K D_{\text{AVE}} + \mathcal{O}(q_1^6 (x - x_0)^6), \tag{6.0.5}$$

and

$$R_2(\Delta) = 1 - \Delta q_2^2 D_{\text{AVE}} + \frac{1}{6}\Delta q_2^4 K D_{\text{AVE}} + \mathcal{O}(q_2^6 (x - x_0)^6). \tag{6.0.6}$$

In fact, assuming that the higher order terms are negligible, D_{AVE} and K are the same for both experiments with different values of q. Rearranging the LHS and RHS in (6.0.5) and (6.0.6) we can compute D_{AVE} and K from R_1 and R_2 respectively. Although more work needs to be done in order to verify the validity of this approach, optimization techniques in DW-MRI experiments for different values of q have been used [3]. This approach makes use of the definition in (4.7.14) that seems to well capture the presence of inhomogeneities (see Section 5.4.2), and it may provide a practical way for the computation of D_{AVE} from the signals. However, further work is required for choosing suitable values for q.

To the best our knowledge, the model proposed in this work has not been used for the simulation of diffusion in heterogenous media in connection with measurements of ADC and we believe that the results are promising. In particular, the model and the source code [9] could be used to measure diffusion in a specific cell-tissue configuration by tuning the physiological parameters. This could be useful for addressing questions and validating results from a standard DW-MRI procedure.

In Figure 6.1, we show the DPDF for the coupled system introduced in Section 4.1. The solution has some expected characteristics; it is discontinuous in the cellular region due to the presence of membranes and is decreases monotonically on the left and on the right (see Figure 6.1a). Figure 6.1b shows the DPDF in the channel of exclusively extracellular space. As expected, the solution in this channel is continuous; this is the result of the absence of cellular barriers in this particular part of the domain. The ADC for this model was not computed. However, due to the presence of more extracellular space, we would expect that information about the size and configuration of cells may be obscured, because a particle, could, theoretically, move across the entire domain

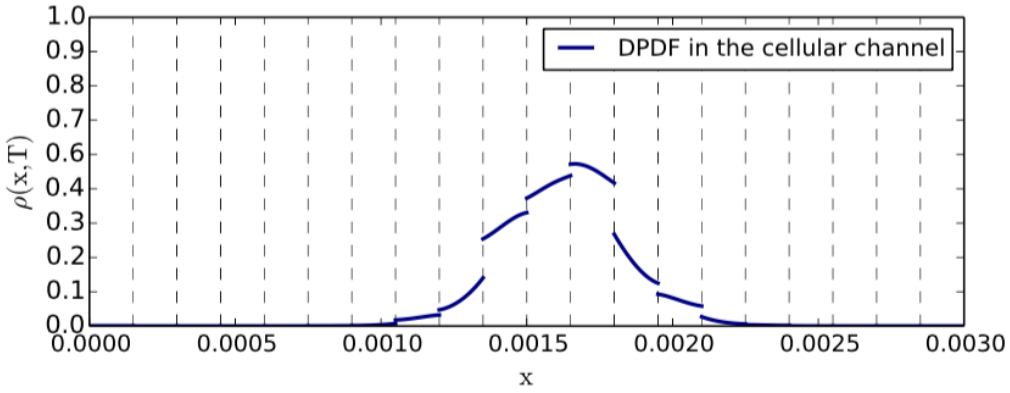

(a)

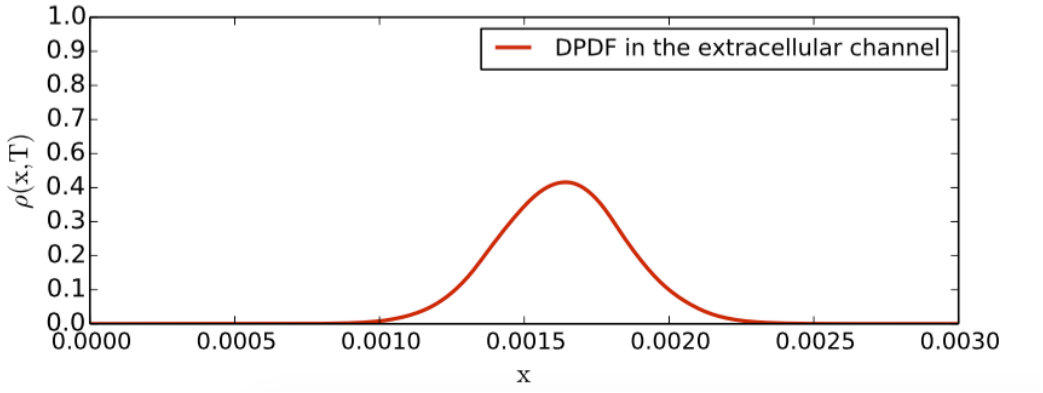

(b)

Figure 6.1: DPDF for the coupled 1D+1D system with the cellular and extracellular channels. Figure 6.1a shows the solution for the coupled system when the molecules start diffusing inside a cell in the cellular channel., Figure 6.1b displays the DPDF for the same particles diffusing in the extracellular channel of just extracellular space.

without crossing any barrier. Thus, in the future, we will use this model to study the robustness of any results we obtain in the model combining only the cellular channel.

Theoretically, the model can be extended to higher dimensions: this would definitely allow for measurements of the ADC for more complete and broader sets of cell configuration and sizes. In the case of a higher dimensional domain, isotropic as well anisotropic diffusion can be measured and we expect to be able to observe the same characteristics in the ADC due to the presence of inhomogeneities as in the one dimensional case.

Bibliography

[1] A. Abragam. *The Principles of Nuclear Magnetism.* Oxford Univerisity Press , London, 1961.

[2] D.C. Alexandre. An Introduction to Computational Diffusion MRI: the Diffusion Tensor and Beyond. In Joachim Weickert and Hans Hagen, editors, *Visualization and Processing of Tensor Fields*, Mathematics and Visualization, pages 83–106. Springer Berlin Heidelberg, 2006.

[3] D.C. Alexandre. Axon radius measurements in vivo fro diffusion MRI: a feasibility study. *IEEE*, 2007.

[4] D.C. Alexandre. A General Framework for Experiment Design in Diffusion MRI and Its Application in Measuring Direct Tissue-Microstructure Features. *Magnetic Resonance in Medicine*, 60:439–448, 2008.

[5] U.M. Ascher L.R.Petzold. *Computer Methods for Ordinary Differential Equations ans Differential-Algebraic Equations.* Society for Industrial and Applied Mathematics, 1998.

[6] P. J. Basser and D. K. Jones. Diffusion Tensor MRI: theory experimental design and data analisys - a technical review theory experimental design and data analisys - a technical review. *NMR in Biomedicine*, 15:456–467, 2002.

[7] P. J. Cameron. Notes on Probability. www.maths.qmul.ac.uk/ pjc/notes/prob.pdf, December 2000.

[8] C.Y. Carr and E. M. Purcell. Effects of Diffusion on Free Precession in Nuclear Magnetic Resonance Experiments. *Physical Review*, 94(630), 1954.

[9] J. Cervi. Source code. https://bitbucket.org/jessicacervi/inhomogeneous_diff_code, July 2015.

[10] GM. Cooper. *The Cell, a Molecular Approach*. Sinauer Associates, 2nd edition, 2000.

[11] A. Einstein. A New Determination of Molecular Dimensions. *Annalen der Physik*, 19:289–306, 1906.

[12] Aaron Szafer et al. Theoretical model for water diffusion in tissues. *MRM*, 33(5):697–712, May 1995.

[13] L. L. Latour et al. Time-dependent diffusion of water in a biological model system. *PNAS*, 91(4):1229–1233, Febraury 1994.

[14] Peter Hagmann et al. Understanding Diffusion MR imaging Techiniques: from scalar Diffusion-Weighted Imaging to Diffusion Tensor Imaging and beyond. *RadioGraphics*, 96(1), October 2006.

[15] J. Gravner. Lecture Notes on Probability Theory. www.math.ucdavis.edu/ gravner/MAT135A/resources/lecturenotes.pdf, January 2014.

[16] O. G. Mouritsen I. Vattulainen. Diffusion in Membranes. In J. Kärger P. Heitjans, editor, *Diffusion in Condensd Matter*, chapter 12, pages 471–509. Springer Berlin Heidelberg, 2005.

[17] M. A. Jacobs et al. Diffusion Weighted Imaging with ADC Mapping and Spectroscopy in Prostate Cancer. *Topics in Magnetic Resonance Imaging*, 19(6):261–272, June 2008.

[18] Jr J.L. Hodges and E.L. Lehmann. *Basic Concepts of Probability and Statistics*. Society for Industrial and Applied Mathematics, 2005.

[19] P.K. Kuchel et al. Stejskal–Tanner Equation Derived in Full. *Concepts in Magnetic Resonance*, 40A(5):205–214, 2012.

[20] D. Le Bihan at al. Diffusion Tensor Imaging: Concepts and Applications. *Journal of Magnetic Resonance Imaging*, 13:534–546, 2001.

[21] R. J. LeVeque. Finite Difference Methods for Differential Equations. http://disciplinas.stoa.usp.br/pluginfile.php/41896/modresource/content/1/LeVeque

[22] L.Zhigilei. Introduction to Atomistic Simulations. http://people.virginia.edu/ lz2n/mse627/notes/Diffusion.pdf.

[23] R. M. M. Mattheij S. W. Rienstra and J. H. M. ten Thije Boonkkamp. *Partial Differential Equation. Modeling, Analysis, Computation.* Society for Industrial and Applied Mathematics, 2005.

[24] S. Mori and J. Zhang. Principles of diffusion tensor imaging ans its applications to basic neuroscience research. *Elsevier*, 51(6):527–539, September 2006.

[25] D.G. Norris. The effects of microscopic tissue paramenters on the diffusion weighted magnetic resonance imaging experiment. *NMR in Biomedicine*, 14:77–93, 2001.

[26] J.F. Nye. *Physical Properties of Crystals: Their Representation by Tensors and Matrices*. Oxford Science Publications, 1999.

[27] T. P. L. Roberts and E. S. Schwartz. Principles and implementation of diffusion-weighted and diffusion tensor imaging. *Pediatric Radiology*, 37:738–749, 2007.

[28] R.M.A. Roque Malherbe. Diffusion in porous materials. In *Adsorption and Diffusion in Nanoporous Materials*. CRC Press, 2007.

[29] R.N. Sener. Diffusion MRI: apparent diffusion coeffient in the normal brain and classification of brain disorder based on ADC values. *Computeritez Medical Imaging and Graphcs*, 25(4):299–326, July 2001.

[30] E. O. Stejskal and J.E. Tanner. Spin diffusion measurements: Spin echoes in the presence of a time dependent field gradient. *The Journal of Chemical Physics*, 42(1):288–292, January 1965.

[31] J. E. Tanner. Transient diffusion in a system partioned by permeable barriers. Application to NMR measurements with a pulsed field gradient. *Journal of Chemical Physics*, 69(4):1748–1754, August 1978.

[32] Walter A. Strauss. *Partial Differential Equation, an Introduction.* John Wiley ans Sons.Wiley, 2nd edition, 2007.

[33] E. X. Wu and M. M. Cheung. MR diffusion kurtosis imaging for neural tissue characterization. *NMR in Biomedicine*, 23(7):836–848, August 2010.

[34] Z-PLiang and P.C.Lauterbur. *Principles of Magnetic Resonance Imaging.* IEEE Press Series in Biomedical Engineering, 2000.

[35] E. Zauderer. *Partial Differential Equation of Applied Mathematics.* John Wiley ans Sons., 2006.

[36] L. Zhigilei. Mobility of atoms and diffusion. einstein relation. http://people.virginia.edu/ lz2n/mse627/notes/Diffusion.pdf, November 1999.